

Consequences of unitary evolution of coupled qubit-resonator systems for stabilizing circuits in surface codes

H.W.L. Naus* and R. Versluis†

*Quantum Technology, TNO, P.O. Box 155, 2600 AD Delft,
The Netherlands and QuTech, Delft University of Technology,
P.O. Box 5046, 2600 GA Delft, The Netherlands*

(Dated: August 28, 2019)

Surface codes based on stabilizer circuits may pave the way for large scale fault-tolerant quantum computation. The surface code, being a fully planar implementation of a larger family of error correction codes, uses only single- and two-qubit gates and the error threshold falls close to 1% for a large range of errors. Among the most promising candidates to physically implement such circuits and codes are superconducting qubits, such as transmons, coupled by resonators to enable the two-qubit interactions. In this study, we investigate a X and Z stabilizing circuit realized by two data qubits, two ancillas and four resonators. The aim is to assess the consequences of unitary evolution of the interacting system, in particular for given stable initial states, on the fidelity of the output states and the probabilities of obtaining the correct error syndrome (capture probabilities). To this end, we model the system with a Jaynes-Tavis-Cummings Hamiltonian and construct the low-excitation level evolution operators. The analysis is limited to two (out of four) stable input states. We assume an ideal system with perfect single- and two-qubit gates, perfect measurements taking zero measurement time and no decoherence or leakage. Our analysis shows that the capture probabilities after the execution of a single stabilizer round are not equal to 100%, but vary between 99.2% and 99.99%. This is caused solely by the unitary evolution of the interacting system. Two consecutive rounds of stabilizer measurements result in capture probability values that depend heavily on the duration of the evolution, but vary between 0% and 99%. Also due to the unitary evolution, the final state of the data qubits leaves the the four-dimensional subspace, which results in a state fidelity oscillating between 0 and 1. Even if an error on the qubits is captured, the correcting operation on the qubit will not bring the qubit to the original state. The errors induced by the Hamiltonian evolution of the system cannot be interpreted nor classified as commonly appearing errors. Additional or augmented quantum error correction is possibly required to compensate these effects of resonator-qubit interaction.

I. INTRODUCTION

In order to perform computations with a gate-based universal quantum computer, quantum error correction is mandatory [1]. Surface codes, operated as stabilizer codes can lead to large scale, fault-tolerant quantum computing [2–4]. The goal is to identify and correct several quantum errors meaning that qubits are not in the state aimed for. Such errors can be caused by environmental decoherence, imperfect knowledge of the quantum system yielding errors in coherent control, imperfect initialization and loss of qubits. Leakage to unwanted states and measurement errors may happen as well. In principle, stabilizer codes indeed can correct such uncorrelated errors. For quantum processors based on superconducting qubits, scalable circuit and control have been recently proposed to execute the error-correction cycles [5].

Superconducting quantum systems are promising candidates for near-term quantum computers [6, 7]. Such devices consist out of transmon(-like) qubits which are coupled by resonators [8, 9]. This coupling is exploited to perform two-qubit gates necessary for universal computing and error-correction codes. It is important to realize

that the qubit-resonator interaction cannot be switched off in the state-of-the-art quantum circuits. It can be made effectively low by detuning the frequencies of qubit and resonators. The near-resonant situation is however necessary to obtain sufficient entanglement for gate operations. Note that the coupling of read-out resonators or cavities can be tuned to low values necessary to obtain the dispersive limit, enabling quantum non-demolition measurements. The situation for electron spin qubits in quantum dots is somewhat different since the exchange interaction between the electrons can be tuned to almost arbitrarily small values.

In this paper, we study the unitary evolution of a four-qubit system coupled by four resonators in the context of a stabilizing circuit. Our specific choice is motivated by the four-qubit X and Z stabilizing circuit proposed in [2]; see also [10]. In contrast with [2], we take into account the unitary evolution of the interacting system of qubits and resonators. The stable two-qubit states are the well-known Bell states. We consider as initial state of the complete system – two data qubits, two ancillas and resonators – a product state of such a Bell state, the corresponding two-ancilla state and empty resonators. The unitary evolution of this state governed by a Jaynes-Tavis-Cummings Hamiltonian is calculated with the techniques of [11]. Consequences for subsequent measurement probabilities and state fidelities are assessed.

* rik.naus@tno.nl

† richard.versluis@tno.nl

Our work is related to the recent gate-error analysis [12], where the dynamics of two transmons coupled by a resonator has been studied in relation to gates implemented by pulses. Systematic errors due to the usually neglected interaction of the total system have been identified. Note that the unitary evolution yields a ‘detrimental effect’ on the computational subspace. We will obtain similar results in the context of a stabilizer circuit and show that the fidelity of a desired (Bell) state in the two data qubit space deteriorates rapidly. These errors cannot be corrected by the stabilizer code under consideration. Recently, a study addressing fault-tolerance by including dynamics in small systems has appeared [13].

The outline of this paper is as follows. The next section presents the X and Z stabilizing circuit as well as the corresponding physical implementation in terms of data qubits, ancillas and resonators. It also explicitly defines the model Hamiltonian and solutions for the lowest excitation subspaces. Subsequently, the unitary evolution of two complete initial states, each containing a stable Bell state, is studied in III. Corresponding fidelities and reinsertion of the final state into the stabilizing circuit are investigated in the sections IV and V. Unitary free evolution and the related transformation to a rotating frame are addressed in VI. It is followed in section VII by a theoretical discussion assessing results and consequences in the context of error analysis, stabilizers and quantum operations. The last section VIII contains conclusions. Note that some adopted definitions and useful relations are given in appendix A.

II. X AND Z STABILIZING CIRCUIT

We consider the X and Z stabilizer circuit as presented in appendix B of [2], however extended with unitary (Hamiltonian) evolution $U(t)$ for time duration t , cf. Figure 1. The ideal quantum circuit does not include U and is part of the in [2-4] outlined surface code. It is built with two data qubits and two ancillas, also called measure qubits. The corresponding measurement result is the *error syndrome* [14].

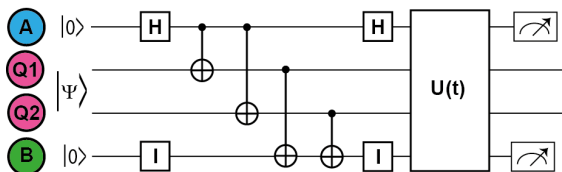


FIG. 1. Quantum X and Z stabilizer circuit including unitary evolution; the ideal circuit does not include $U(t)$.

A. Circuit analysis

The ideal circuit is analyzed by [2] in terms of the standard (computational) basis. For convenience, we repeat the analysis in terms of the Bell states in appendix B. In both ways it is demonstrated that the two data qubits are stabilized in a simultaneous eigenstate of $X^{[1]}X^{[2]}$ and $Z^{[1]}Z^{[2]}$. These are exactly the Bell states:

$$\begin{aligned} X^{[1]}X^{[2]}|\Phi^+\rangle &= |\Phi^+\rangle, & X^{[1]}X^{[2]}|\Psi^+\rangle &= |\Psi^+\rangle, \\ X^{[1]}X^{[2]}|\Phi^-\rangle &= -|\Phi^-\rangle, & X^{[1]}X^{[2]}|\Psi^-\rangle &= -|\Psi^-\rangle, \\ Z^{[1]}Z^{[2]}|\Phi^+\rangle &= |\Phi^+\rangle, & Z^{[1]}Z^{[2]}|\Psi^+\rangle &= -|\Psi^+\rangle, \\ Z^{[1]}Z^{[2]}|\Phi^-\rangle &= |\Phi^-\rangle, & Z^{[1]}Z^{[2]}|\Psi^-\rangle &= -|\Psi^-\rangle. \end{aligned} \quad (1)$$

In other words, if we select one of these states as input to the circuit, it can readily be verified that the same output state is obtained. The result of the ancilla measurement, the error syndrome, is reproduced as well with probability one. Thus we have shown that this indeed is a stabilizer circuit.

B. Error correction

Assume that we put a stable state into the circuit. As mentioned above, without errors, the ancilla measurement result is known. Suppose, however, that due to some error a different error syndrome is obtained. Concomitantly, the resulting two-qubit state has changed as well. Because the final state is nevertheless known, error correction by applying one or two single qubit operations is possible. We work out this procedure for two out of four cases, thereby explicitly constructing the necessary operations. Equations (A.2, A.3) are repeatedly used.

- State $|\Phi^+\rangle$
Error syndrome $(+1, +1)$, that is no errors are detected; otherwise:
 - Error syndrome $(-1, +1)$, state $|\Phi^-\rangle$, correction $Z^{[1]}|\Phi^-\rangle = |\Phi^+\rangle$.
 - Error syndrome $(+1, -1)$, state $|\Psi^+\rangle$, correction $X^{[2]}|\Psi^+\rangle = |\Phi^+\rangle$.
 - Error syndrome $(-1, -1)$, state $|\Psi^-\rangle$, correction $X^{[2]}Z^{[1]}|\Psi^-\rangle = |\Phi^+\rangle$.
- State $|\Psi^+\rangle$
Error syndrome $(+1, -1)$, that is no errors are detected; otherwise:
 - Error syndrome $(+1, +1)$, state $|\Phi^+\rangle$, correction $X^{[1]}|\Phi^+\rangle = |\Psi^+\rangle$.
 - Error syndrome $(-1, +1)$, state $|\Phi^-\rangle$, correction $X^{[2]}Z^{[1]}|\Phi^-\rangle = |\Psi^+\rangle$.
 - Error syndrome $(-1, -1)$, state $|\Psi^-\rangle$, correction $Z^{[1]}|\Psi^-\rangle = |\Psi^+\rangle$.

Note that these error corrections are not unique, for example $Z^{[2]}|\Phi^-\rangle = |\Phi^+\rangle$.

C. Dynamics

Two data qubits stabilized by one measure- X qubit A and one measure- Z qubit B [2] coupled by resonators are shown and labelled in Figure 2.

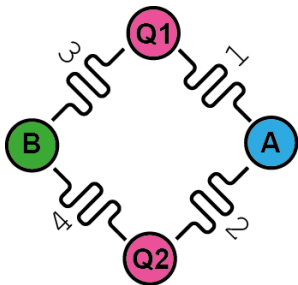


FIG. 2. Two data qubits and two ancillas coupled by four resonators.

The generalized Jaynes-Tavis-Cummings Hamiltonian for this system is given by [11]

$$H = H_0^q + H_0^r + H_{\text{int}}^{11} + H_{\text{int}}^{1a} + H_{\text{int}}^{2a} + H_{\text{int}}^{22} + H_{\text{int}}^{31} + H_{\text{int}}^{3b} + H_{\text{int}}^{4b} + H_{\text{int}}^{42}, \quad (2)$$

with the ‘free’ qubit Hamiltonian

$$H_0^q = -\frac{1}{2}\omega'_1\sigma_z^{[1]} - \frac{1}{2}\omega_a\sigma_z^{[a]} - \frac{1}{2}\omega'_2\sigma_z^{[2]} - \frac{1}{2}\omega_b\sigma_z^{[b]} \quad (3)$$

and the Hamiltonian of the resonators

$$H_0^r = \omega_1(a_1^\dagger a_1 + \frac{1}{2}) + \omega_2(a_2^\dagger a_2 + \frac{1}{2}) + \omega_3(a_3^\dagger a_3 + \frac{1}{2}) + \omega_4(a_4^\dagger a_4 + \frac{1}{2}). \quad (4)$$

The interaction terms in the rotating wave approximation read

$$H_{\text{int}}^{11} = g_{11} \left(a_1^\dagger \sigma_+^{[1]} + a_1 \sigma_-^{[1]} \right), \\ H_{\text{int}}^{1a} = g_{1a} \left(a_1^\dagger \sigma_+^{[a]} + a_1 \sigma_-^{[a]} \right), \quad \text{etc.} \quad (5)$$

The frequencies are denoted by $\omega_k, k = 1, \dots, 4$, for the resonators, ω'_1, ω'_2 for the data qubits and ω_a, ω_b for the ancillas. The coupling constants are taken as $g_{11}, g_{1a}, g_{2a}, g_{22}, g_{42}, g_{4b}, g_{3b}, g_{31}$.

To study the dynamics, it is necessary to solve the Schrödinger equation, that is obtaining eigenenergies and eigenstates of the Hamiltonian. Herewith the evolution operator $U(t)$ is constructed. The technique of [11] is applied, where excitation number operators for Jaynes-Tavis-Cummings Hamiltonians are exploited. For the system under consideration this operator \mathcal{N} is given by

$$\mathcal{N} = \sum_{k=1}^4 a_k^\dagger a_k - \frac{1}{2}(\sigma_z^{[1]} + \sigma_z^{[2]} + \sigma_z^{[a]} + \sigma_z^{[b]}). \quad (6)$$

It commutes with the Hamiltonian: $[\mathcal{N}, H] = 0$. Consequently, it is conserved and \mathcal{N} and H can be diagonalized

simultaneously. Thus the dynamics can be analyzed separately for each excitation level.

The eigenstates of the excitation number operator are product states $|r_1, r_2, r_3, r_4\rangle \otimes |q_1, q_2\rangle \otimes |q_a, q_b\rangle$, with $r_k = 0, 1, 2, \dots$ for $k = 1, 2, 3, 4$ and $q_j = \mathbf{0}, \mathbf{1}$ for $j = 1, 2, a, b$. The lowest level \mathcal{N} state is also the ground state of the Hamiltonian

$$|E_0\rangle = |0, 0, 0, 0\rangle \otimes |\mathbf{0}, \mathbf{0}\rangle \otimes |\mathbf{0}, \mathbf{0}\rangle, \quad (7)$$

with energy eigenvalue

$$E_0 = \frac{1}{2}(\omega_1 + \omega_2 + \omega_3 + \omega_4 - \omega'_1 - \omega'_2 - \omega_a - \omega_b). \quad (8)$$

The first excitation level is eight-fold degenerate with respect to \mathcal{N} ; we choose the basis states as given in appendix C. The matrix elements of the Hamiltonian in this subspace $\mathcal{H}_{ij}, i, j = 1, 2, \dots, 8$ are also listed in appendix C. The corresponding eigenvalue problem needs to be solved:

$$\mathcal{H}a_{1\mu} = E_{1\mu}a_{1\mu}, \quad \mu = 1, 2, \dots, 8. \quad (9)$$

As in [11], this is done by means of the Jacobi method. In this way, we obtain the eigenstates

$$|E_{1\mu}\rangle = \sum_{k=1}^8 a_{\mu k} |e_k\rangle \quad (10)$$

and the subspace evolution operator

$$U_1(t) = \sum_{\mu=1}^8 e^{-iE_{1\mu}t} |E_{1\mu}\rangle \langle E_{1\mu}|. \quad (11)$$

We proceed to the second excitation level which has dimension thirty-two. See appendix C for our choice of basis states $|f_k\rangle$. The matrix elements in the second excitation subspace $H_{kl}, k, l = 1, 2, \dots, 32$ are explicitly given in appendix C as well. The eigenvalue problem in this subspace

$$Hb_\eta = E_{2\eta}b_\eta, \quad \eta = 1, 2, \dots, 32, \quad (12)$$

is again solved with the Jacobi method. It yields the eigenstates

$$|E_{2\eta}\rangle = \sum_{l=1}^{32} b_{\eta l} |f_l\rangle \quad (13)$$

and the second excitation subspace evolution operator

$$U_2(t) = \sum_{\eta=1}^{32} e^{-iE_{2\eta}t} |E_{2\eta}\rangle \langle E_{2\eta}|. \quad (14)$$

The constructed evolution operators will be used to compute specific unitary evolutions.

III. UNITARY EVOLUTION

In this paper, we presuppose that the X and Z stabilizing circuit is ideal up to and including the last Hadamard operation, step 7. in appendix B. If one of the stable Bell states (A.1) has been put in, it is reproduced in (B.9) because the corresponding coefficient is one and the others are zero. Before completing the circuit by measuring the ancillas we now assume unitary evolution governed by the complete Hamiltonian and analyze the consequences. This is done for two initial states, containing the Bell states $|\Phi^+\rangle$ and $|\Psi^+\rangle$. Assuming empty resonators, only the ground state and the second excitation subspace need to be taken into account. In principle, the analysis for the states $|\Phi^-\rangle$ and $|\Psi^-\rangle$ proceeds analogously. The corresponding states, however, have components in the third excitation subspace which makes computations more cumbersome. Therefore, we restrict ourselves to $|\Phi^+\rangle$ and $|\Psi^+\rangle$.

A. Bell state $|\Phi^+\rangle$

First, we assume that the two-qubit Bell state $|\Phi^+\rangle$ has been put in the ideal stabilizer circuit. Then we study unitary evolution of the system after the last Hadamard operation has been performed. Thus the ‘initial’ state follows from (B.9) with $A_+ = 1, B_+ = A_- = B_- = 0$ and the inclusion with resonators, presumed to be empty

$$|\varphi_0\rangle = |0, 0, 0, 0\rangle \otimes |\Phi^+\rangle \otimes |\mathbf{0}, \mathbf{0}\rangle. \quad (15)$$

In terms of the defined basis vectors we get a superposition of the ground state and a state in the second excitation subspace

$$|\varphi_0\rangle = \frac{1}{\sqrt{2}}\sqrt{2}(|E_0\rangle + |f_{27}\rangle). \quad (16)$$

Its unitary evolution is therefore given by

$$\begin{aligned} |\varphi(t)\rangle &= (U_0(t) + U_1(t) + U_2(t) + \dots) |\varphi_0\rangle \\ &= \frac{1}{\sqrt{2}}\sqrt{2} (U(t)|E_0\rangle + U_2(t)|f_{27}\rangle) \\ &= \frac{1}{\sqrt{2}}\sqrt{2} \left(e^{-iE_0t}|E_0\rangle + \sum_{\eta=1}^{32} e^{-iE_{2\eta}t} b_{\eta 27} |E_{2\eta}\rangle \right) \\ &= \frac{1}{\sqrt{2}}\sqrt{2} \left(e^{-iE_0t}|E_0\rangle + \sum_{\eta=1}^{32} \sum_{k=1}^{32} e^{-iE_{2\eta}t} b_{\eta 27} b_{\eta k} |f_k\rangle \right) \\ &= \frac{1}{\sqrt{2}}\sqrt{2} e^{-iE_0t}|E_0\rangle + \sum_{k=1}^{32} \beta_k(t) |f_k\rangle, \end{aligned} \quad (17)$$

where we have defined

$$\beta_k(t) = \frac{1}{\sqrt{2}}\sqrt{2} \sum_{\eta=1}^{32} e^{-iE_{2\eta}t} b_{\eta 27} b_{\eta k}. \quad (18)$$

At this point we fix the time t and perform the measurement on the ancillas. The measurement operator corresponding to the error syndrome $(+1, +1)$ reads

$$P_{1,1} = \mathcal{I}_{r_1} \otimes \mathcal{I}_{r_2} \otimes \mathcal{I}_{r_3} \otimes \mathcal{I}_{r_4} \otimes \mathcal{I}_{12} \otimes |\mathbf{0}\rangle\langle\mathbf{0}| \otimes |\mathbf{0}\rangle\langle\mathbf{0}|, \quad (19)$$

with identity operators $\mathcal{I}_{r_j}, \mathcal{I}_{12} = \mathcal{I}^{[1]} \otimes \mathcal{I}^{[2]}$. The probability that this result is obtained follows as

$$p(1, 1) = \frac{1}{2} + \sum_{k \in S(1,1)} \beta_k^*(t) \beta_k(t), \quad (20)$$

where the integer set is given as

$$S(1, 1) = \{1, 2, \dots, 12, 15, 16, 19, 20, 23, 24, 27\}. \quad (21)$$

This result is depicted in Figure (3).

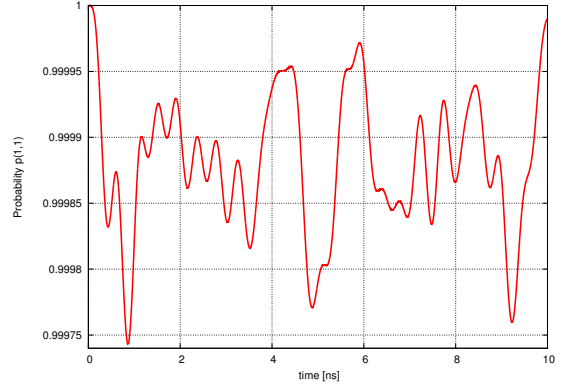


FIG. 3. Probability for obtaining the error syndrome $(1,1)$ after unitary evolution of the state $|0, 0, 0, 0\rangle|\Phi^+\rangle|\mathbf{0}, \mathbf{0}\rangle$ as a function of time. Parameters: $f_1 = 8.14, f_2 = 8.18, f_3 = 8.1, f_4 = 8.06, f'_1 = 6.6, f'_2 = 6.4, f_a = 5.9, f_b = 5.7, g_{11} = 0.51, g_{22} = 0.52, g_{1a} = 0.53, g_{2a} = 0.54, g_{42} = 0.5, g_{4b} = 0.49, g_{3b} = 0.48, g_{31} = 0.47$; all values are given in GHz.

The state after projection and normalization follows as

$$|\varphi_{1,1}\rangle = \frac{1}{\sqrt{p(1,1)}} \left(\frac{1}{\sqrt{2}}\sqrt{2} e^{-iE_0t} |E_0\rangle + \sum_{k \in S(1,1)} \beta_k(t) |f_k\rangle \right). \quad (22)$$

It can be written as a tensor product by factoring out the ancilla states

$$|\varphi_{1,1}\rangle = |\tilde{\varphi}_{1,1}\rangle \otimes |\mathbf{0}\rangle \otimes |\mathbf{0}\rangle. \quad (23)$$

The data qubits–resonators state, however, is still entangled.

We continue with measurements which indicate an error in the state. If the error syndrome equals $(-1, 1)$, the corresponding measurement operator is given by

$$P_{-1,1} = \mathcal{I}_{r_1} \otimes \mathcal{I}_{r_2} \otimes \mathcal{I}_{r_3} \otimes \mathcal{I}_{r_4} \otimes \mathcal{I}_{12} \otimes |\mathbf{1}\rangle\langle\mathbf{1}| \otimes |\mathbf{0}\rangle\langle\mathbf{0}|. \quad (24)$$

We obtain for the probability to find this result

$$p(-1, 1) = \sum_{k \in S(-1,1)} \beta_k^*(t) \beta_k(t), \quad (25)$$

with concomitant normalized state

$$|\varphi_{-1,1}\rangle = \frac{1}{\sqrt{p(-1,1)}} \sum_{k \in S(-1,1)} \beta_k(t) |f_k\rangle \quad (26)$$

and the set

$$S(-1, 1) = \{13, 17, 21, 25, 28, 30\}. \quad (27)$$

The result for the probability is shown in Figure (4). The ancilla states can again be factored out

$$|\varphi_{-1,1}\rangle = |\tilde{\varphi}_{-1,1}\rangle \otimes |\mathbf{1}\rangle \otimes |\mathbf{0}\rangle \quad (28)$$

but data qubits and resonators remain entangled.

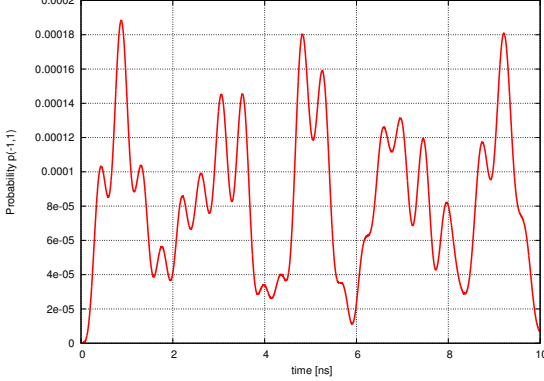


FIG. 4. Probability for obtaining the error syndrome $(-1,1)$ after unitary evolution of the state $|0,0,0,0\rangle|\Phi^+\rangle|\mathbf{0},\mathbf{0}\rangle$ as a function of time. Parameters as in the previous figure.

The analogous results for obtaining the error syndrome $(1, -1)$ are

$$P_{1,-1} = \mathcal{I}_{r_1} \otimes \mathcal{I}_{r_2} \otimes \mathcal{I}_{r_3} \otimes \mathcal{I}_{r_4} \otimes \mathcal{I}_{12} \otimes |\mathbf{0}\rangle\langle\mathbf{0}| \otimes |\mathbf{1}\rangle\langle\mathbf{1}|, \quad (29)$$

with probability

$$p(1, -1) = \sum_{k \in S(1,-1)} \beta_k^*(t) \beta_k(t), \quad (30)$$

state

$$|\varphi_{1,-1}\rangle = \frac{1}{\sqrt{p(1,-1)}} \sum_{k \in S(1,-1)} \beta_k(t) |f_k\rangle, \quad (31)$$

and integer set

$$S(1, -1) = \{14, 18, 22, 26, 29, 31\}. \quad (32)$$

After amputating the ancillas, the state reads

$$|\varphi_{1,-1}\rangle = |\tilde{\varphi}_{1,-1}\rangle \otimes |\mathbf{0}\rangle \otimes |\mathbf{1}\rangle. \quad (33)$$

Since $p(1, -1) < 10^{-4}$, it is not shown.

The error syndrome $(-1, -1)$ corresponds to the operator

$$P_{-1,-1} = \mathcal{I}_{r_1} \otimes \mathcal{I}_{r_2} \otimes \mathcal{I}_{r_3} \otimes \mathcal{I}_{r_4} \otimes \mathcal{I}_{12} \otimes |\mathbf{1}\rangle\langle\mathbf{1}| \otimes |\mathbf{1}\rangle\langle\mathbf{1}|, \quad (34)$$

which projects to one basis state

$$|\varphi_{-1,-1}\rangle = \frac{\beta_{32}(t)}{|\beta_{32}(t)|} |f_{32}\rangle, \quad (35)$$

with probability

$$p(-1, -1) = \beta_{32}^*(t) \beta_{32}(t). \quad (36)$$

This probability is less than 10^{-7} . The final state is a product state in all degrees of freedom

$$|\varphi_{-1,-1}\rangle = |0\rangle \otimes |0\rangle \otimes |0\rangle \otimes |0\rangle \otimes |\mathbf{0}\rangle \otimes |\mathbf{0}\rangle \otimes |\mathbf{1}\rangle \otimes |\mathbf{1}\rangle, \quad (37)$$

where we have omitted a phase factor.

B. Bell state $|\Psi^+\rangle$

We do a similar analysis for the Bell state $|\Psi^+\rangle$:

$$\begin{aligned} |\psi_0\rangle &= |0, 0, 0, 0\rangle \otimes |\Psi^+\rangle \otimes |\mathbf{0}, \mathbf{1}\rangle \\ &= \frac{1}{\sqrt{2}} \sqrt{2} (|f_{29}\rangle + |f_{31}\rangle). \end{aligned} \quad (38)$$

Unitary evolution is governed by $U_2(t)$ and it yields

$$\begin{aligned} |\psi(t)\rangle &= \frac{1}{\sqrt{2}} \sqrt{2} U_2(t) (|f_{29}\rangle + |f_{31}\rangle) \\ &= \frac{1}{\sqrt{2}} \sqrt{2} \sum_{\eta=1}^{32} e^{-iE_{2\eta}t} (b_{\eta 29} + b_{\eta 31}) |E_{2\eta}\rangle \\ &= \frac{1}{\sqrt{2}} \sqrt{2} \sum_{\eta=1}^{32} \sum_{k=1}^{32} e^{-iE_{2\eta}t} (b_{\eta 29} + b_{\eta 31}) b_{\eta k} |f_k\rangle \\ &= \sum_{k=1}^{32} \gamma_k(t) |f_k\rangle, \end{aligned} \quad (39)$$

where we have abbreviated

$$\gamma_k(t) = \frac{1}{\sqrt{2}} \sqrt{2} \sum_{\eta=1}^{32} e^{-iE_{2\eta}t} (b_{\eta 29} + b_{\eta 31}) b_{\eta k}. \quad (40)$$

At this instant of time t the measurement on the ancillas is done. The measurements operators are defined above. The error syndrome corresponding to no error detection reads $(1, -1)$. We obtain for the probability for obtaining these values

$$p(1, -1) = \sum_{k \in S(1,-1)} \gamma_k^*(t) \gamma_k(t), \quad (41)$$

as shown in Figure (5). In order not to overload the notation we do *not* introduce a different symbol for probabilities in different examples. The corresponding normalized state is

$$|\psi_{1,-1}\rangle = \frac{1}{\sqrt{p(1,-1)}} \sum_{k \in S(1,-1)} \gamma_k(t) |f_k\rangle. \quad (42)$$

The ancilla states can of course be separated

$$|\psi_{1,-1}\rangle = |\tilde{\psi}_{1,-1}\rangle \otimes |\mathbf{0}\rangle \otimes |\mathbf{1}\rangle \quad (43)$$

but once more the data qubits and resonators remain entangled.

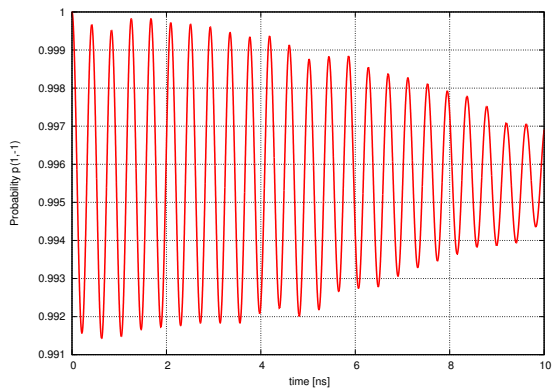


FIG. 5. Probability for obtaining the error syndrome (1,-1) after unitary evolution of the state $|0,0,0,0\rangle|\Psi^+\rangle|\mathbf{0},\mathbf{1}\rangle$ as a function of time. Parameters as in Figure (3).

The expressions for obtaining error syndromes indicating an error can be derived analogously and we merely present these without further comments:

$$p(1,1) = \sum_{k \in S(1,1)} \gamma_k^*(t) \gamma_k(t), \quad (44)$$

$$\begin{aligned} |\psi_{1,1}\rangle &= \frac{1}{\sqrt{p(1,1)}} \sum_{k \in S(1,1)} \gamma_k(t) |f_k\rangle \\ &= |\tilde{\psi}_{1,1}\rangle \otimes |\mathbf{0}\rangle \otimes |\mathbf{0}\rangle. \end{aligned} \quad (45)$$

Figure (6) depicts the probability $p(1,1)$.

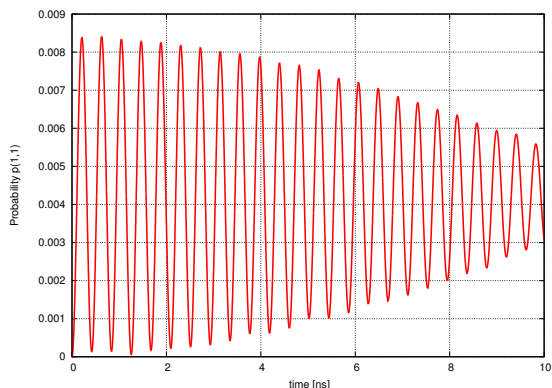


FIG. 6. Probability for obtaining the error syndrome (1,1) after unitary evolution of the state $|0,0,0,0\rangle|\Psi^+\rangle|\mathbf{0},\mathbf{1}\rangle$ as a function of time. Parameters as in Figure (3).

For the error syndrome (-1,1) we get

$$p(-1,1) = \sum_{k \in S(-1,1)} \gamma_k^*(t) \gamma_k(t), \quad (46)$$

$$\begin{aligned} |\psi_{-1,1}\rangle &= \frac{1}{\sqrt{p(-1,1)}} \sum_{k \in S(-1,1)} \gamma_k(t) |f_k\rangle \\ &= |\tilde{\psi}_{-1,1}\rangle \otimes |\mathbf{1}\rangle \otimes |\mathbf{0}\rangle. \end{aligned} \quad (47)$$

Because $p(-1,1) < 10^{-5}$ it is not shown.

Finally, we obtain for the syndrome (-1,-1)

$$p(-1,-1) = \gamma_{32}^*(t) \gamma_{32}(t), \quad (48)$$

which is less than 10^{-3} . The final state

$$|\psi_{-1,-1}\rangle = \frac{1}{\sqrt{p(-1,-1)}} \gamma_{32}(t) |f_{32}\rangle \quad (49)$$

coincides -up to a phase factor- with (37).

IV. FIDELITIES AND ERROR CORRECTION

In the last section, we have analyzed the four-qubit stabilizer system. Unitary evolution of the complete coupled system initially containing a separable stable Bell state has been calculated. There are two cases to be distinguished on the basis of the found error syndrome. In the first one, the syndrome indicates no error is and hence no error correction is applied. Secondly, the syndrome indicates a specific error which subsequently may be corrected by applying the correction operators on the data qubits, cf. section (IIB). In both cases, one then is interested in a measure how well the stabilizer performs. Note that in all cases the desired stable two-qubit state, or ‘target state’, is known. Thus a natural choice would be the fidelity of the realized state. We have seen that in most cases, however, the two data qubits and the resonators are entangled and the concomitant two-qubit state is not defined. As a consequence, one needs to exploit the density matrix formalism [14, 15] and the technique of partial tracing. The latter reduces the density matrix of a composite system to the density matrix of a subsystem by performing the partial trace over the other degrees of freedom. The reduced density matrix of the data qubits is therefore obtained by tracing out the resonator degrees of freedom. Note, however, in case of entanglement the resulting subsystem density matrix will *not* correspond to a pure state. In our examples, the resonators-qubits state is of course pure and, with the exception of the product state after obtaining the error syndrome (-1,-1), entangled. Consequently, we cannot identify a pure two-qubit state since the density matrix corresponds to a mixed state. Nevertheless, we can use the concept of the fidelity between a pure (target) state $|\psi\rangle$ and the mixed state described by a density operator ρ . It is defined as

$$F(|\psi\rangle, \rho) = \sqrt{\langle \psi | \rho | \psi \rangle}, \quad (50)$$

cf. [8, 14].

A. Density matrix: Bell state $|\Phi^+\rangle$

Once more we start the analysis for the case of the error syndrome (1,1). The state after having factored

out the ancillas (23) is rewritten as

$$|\tilde{\phi}_{1,1}\rangle = \frac{1}{\sqrt{p(1,1)}} \sum_{k \in \tilde{S}} \beta_k(t) |\tilde{f}_k\rangle, \quad (51)$$

thereby (implicitly) defining $|\tilde{f}_k\rangle$, $\beta_0(t) = \frac{1}{2}\sqrt{2}e^{-iE_0t}$ and $\tilde{S} = \{0\} \cup S(1,1)$. The concomitant density matrix is

therefore

$$\rho = \frac{1}{p(1,1)} \sum_{k \in \tilde{S}} \sum_{l \in \tilde{S}} \beta_k(t) \beta_l^*(t) |\tilde{f}_k\rangle \langle \tilde{f}_l|. \quad (52)$$

At this point we take the partial trace with respect to the resonator degrees of freedom. The result for the reduced data qubit density operator is given by

$$\begin{aligned} \rho_q = \frac{1}{p(1,1)} & \left\{ \sum_{k=0}^{10} \beta_k^*(t) \beta_k(t) |\mathbf{0}, \mathbf{0}\rangle \langle \mathbf{0}, \mathbf{0}| + \beta_{27}^*(t) \beta_{27}(t) |\mathbf{1}, \mathbf{1}\rangle \langle \mathbf{1}, \mathbf{1}| \right. \\ & + \sum_{k=11,15,19,23} \beta_k^*(t) \beta_k(t) |\mathbf{1}, \mathbf{0}\rangle \langle \mathbf{1}, \mathbf{0}| + \sum_{k=12,16,20,24} \beta_k^*(t) \beta_k(t) |\mathbf{0}, \mathbf{1}\rangle \langle \mathbf{0}, \mathbf{1}| \\ & + \beta_0(t) \beta_{27}^*(t) |\mathbf{0}, \mathbf{0}\rangle \langle \mathbf{1}, \mathbf{1}| + \beta_{27}(t) \beta_0^*(t) |\mathbf{1}, \mathbf{1}\rangle \langle \mathbf{0}, \mathbf{0}| \\ & + (\beta_{11}(t) \beta_{12}^*(t) + \beta_{15}(t) \beta_{16}^*(t) + \beta_{19}(t) \beta_{20}^*(t) + \beta_{23}(t) \beta_{24}^*(t)) |\mathbf{1}, \mathbf{0}\rangle \langle \mathbf{0}, \mathbf{1}| \\ & \left. + (\beta_{12}(t) \beta_{11}^*(t) + \beta_{16}(t) \beta_{15}^*(t) + \beta_{20}(t) \beta_{19}^*(t) + \beta_{24}(t) \beta_{23}^*(t)) |\mathbf{0}, \mathbf{1}\rangle \langle \mathbf{1}, \mathbf{0}| \right\}. \end{aligned} \quad (53)$$

We eventually obtain the fidelity

$$F(|\Phi^+\rangle, \rho_q) = \sqrt{\langle \Phi^+ | \rho_q | \Phi^+ \rangle} = \left\{ \frac{1}{2p(1,1)} \left[\sum_{k=0}^{10} \beta_k^*(t) \beta_k(t) + \beta_{27}^*(t) \beta_{27}(t) + \beta_0^*(t) \beta_{27}(t) + \beta_{27}^*(t) \beta_0(t) \right] \right\}^{1/2},$$

which is shown in Figure (7).

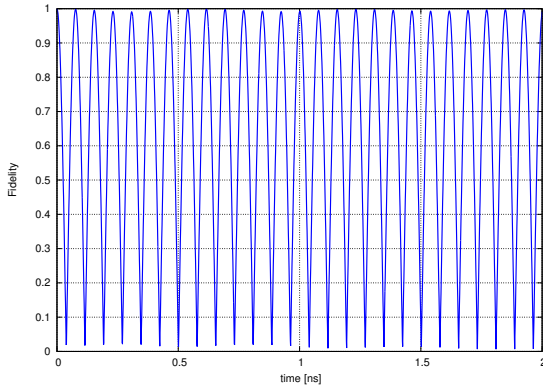


FIG. 7. Fidelity as a function of time after unitary evolution of the state $|0,0,0,0\rangle|\Phi^+\rangle|\mathbf{0},\mathbf{0}\rangle$ and subsequently obtaining error syndrome $(1,1)$. Parameters as in Figure (3).

After having detected an error, one may apply a correction operator to the state. We analyze the consequences by computing the fidelity of the obtained target state and the reduced density operator. Since the partial trace is taken with respect to the resonators degrees of freedom and the error correction only operates on the data qubits, we can first compute the reduced density matrix

and eventually apply the error correction operator on the target state. We demonstrate the method for the various error syndromes indicating an error.

For the syndrome $(-1,1)$ the state after factoring out the ancillas reads

$$|\tilde{\phi}_{-1,1}\rangle = \frac{1}{\sqrt{p(-1,1)}} \sum_{k \in S(-1,1)} \beta_k(t) |\tilde{f}_k\rangle, \quad (54)$$

with corresponding density matrix

$$\rho = \frac{1}{p(-1,1)} \sum_{k \in S(-1,1)} \sum_{l \in S(-1,1)} \beta_k(t) \beta_l^*(t) |\tilde{f}_k\rangle \langle \tilde{f}_l|. \quad (55)$$

The reduced qubit density matrix follows as

$$\begin{aligned} \rho_q = \frac{1}{p(-1,1)} & \left\{ \sum_{k=13,17,21,25} \beta_k^*(t) \beta_k(t) |\mathbf{0}, \mathbf{0}\rangle \langle \mathbf{0}, \mathbf{0}| \right. \\ & + \beta_{28}(t) \beta_{28}^*(t) |\mathbf{1}, \mathbf{0}\rangle \langle \mathbf{1}, \mathbf{0}| + \beta_{30}(t) \beta_{30}^*(t) |\mathbf{0}, \mathbf{1}\rangle \langle \mathbf{0}, \mathbf{1}| \\ & \left. + \beta_{28}(t) \beta_{30}^*(t) |\mathbf{1}, \mathbf{0}\rangle \langle \mathbf{0}, \mathbf{1}| + \beta_{30}(t) \beta_{28}^*(t) |\mathbf{0}, \mathbf{1}\rangle \langle \mathbf{1}, \mathbf{0}| \right\}. \end{aligned} \quad (56)$$

Herewith we get as fidelity

$$\begin{aligned}
F(|\Phi^+\rangle, Z^{[1]}\rho_q Z^{[1]}) &= \sqrt{\langle \Phi^+ | Z^{[1]}\rho_q Z^{[1]} | \Phi^+ \rangle} = \sqrt{\langle \Phi^- | \rho_q | \Phi^- \rangle} \\
&= \left\{ \frac{1}{2p(-1,1)} \left[\beta_{13}^*(t)\beta_{13}(t) + \beta_{17}^*(t)\beta_{17}(t) + \beta_{21}^*(t)\beta_{21}(t) + \beta_{25}^*(t)\beta_{25}(t) \right] \right\}^{1/2}, \tag{57}
\end{aligned}$$

which is close to zero.

Analogously, for the error syndrome $(1, -1)$ the state after factoring out the ancillas is given by

$$|\tilde{\phi}_{1,-1}\rangle = \frac{1}{\sqrt{p(1,-1)}} \sum_{k \in S(1,-1)} \beta_k(t) |\tilde{f}_k\rangle, \tag{58}$$

with concomitant density matrix

$$\rho = \frac{1}{p(1,-1)} \sum_{k \in S(1,-1)} \sum_{l \in S(1,-1)} \beta_k(t) \beta_l^*(t) |\tilde{f}_k\rangle \langle \tilde{f}_l|. \tag{59}$$

Calculating the partial trace yields

$$\begin{aligned}
\rho_q &= \frac{1}{p(1,-1)} \left\{ \sum_{k=14,18,22,26} \beta_k^*(t)\beta_k(t) |\mathbf{0}, \mathbf{0}\rangle \langle \mathbf{0}, \mathbf{0}| + \beta_{29}(t)\beta_{29}^*(t) |\mathbf{1}, \mathbf{0}\rangle \langle \mathbf{1}, \mathbf{0}| + \beta_{31}(t)\beta_{31}^*(t) |\mathbf{0}, \mathbf{1}\rangle \langle \mathbf{0}, \mathbf{1}| \right. \\
&\quad \left. + \beta_{29}(t)\beta_{31}^*(t) |\mathbf{1}, \mathbf{0}\rangle \langle \mathbf{0}, \mathbf{1}| + \beta_{31}(t)\beta_{29}^*(t) |\mathbf{0}, \mathbf{1}\rangle \langle \mathbf{1}, \mathbf{0}| \right\}. \tag{60}
\end{aligned}$$

Subsequently, we obtain the fidelity

$$\begin{aligned}
F(|\Phi^+\rangle, X^{[2]}\rho_q X^{[2]}) &= \sqrt{\langle \Phi^+ | X^{[2]}\rho_q X^{[2]} | \Phi^+ \rangle} = \sqrt{\langle \Psi^+ | \rho_q | \Psi^+ \rangle} \\
&= \left\{ \frac{1}{2p(1,-1)} \left[\beta_{29}^*(t)\beta_{29}(t) + \beta_{31}^*(t)\beta_{31}(t) + \beta_{31}^*(t)\beta_{29}(t) + \beta_{29}^*(t)\beta_{31}(t) \right] \right\}^{1/2}, \tag{61}
\end{aligned}$$

as shown in Figure (8).

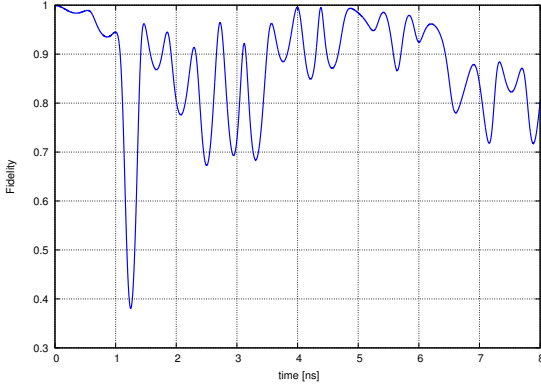


FIG. 8. Fidelity as a function of time after unitary evolution of the state $|0,0,0,0\rangle|\Phi^+\rangle|\mathbf{0}, \mathbf{0}\rangle$, subsequently obtaining error syndrome $(1, -1)$ and error correction. Parameters as in Figure (3).

In case of error syndrome $(-1, -1)$, it is easily seen that the reduced density matrix corresponds to a the pure state

$$\rho_q = |\mathbf{0}, \mathbf{0}\rangle \langle \mathbf{0}, \mathbf{0}|. \tag{62}$$

Then we get

$$\begin{aligned}
&F(|\Phi^+\rangle, X^{[2]}Z^{[1]}\rho_q Z^{[1]}X^{[2]}) \\
&= \sqrt{\langle \Phi^+ | Z^{[1]}X^{[2]}\rho_q Z^{[1]}X^{[2]} | \Phi^+ \rangle} \\
&= \sqrt{\langle \Psi^- | \rho_q | \Psi^- \rangle} = 0, \tag{63}
\end{aligned}$$

that is a vanishing fidelity.

B. Density matrix: Bell state $|\Psi^+\rangle$

The computations for the Bell state $|\Psi^+\rangle$ of course proceed completely analogously and we merely present the results for the obtained fidelities. For the error syndrome $(1, -1)$, we get

$$F(|\Psi^+\rangle, \rho_q) = \sqrt{\langle \Psi^+ | \rho_q | \Psi^+ \rangle} = \left\{ \frac{1}{2p(1,-1)} \left[\gamma_{29}^*(t)\gamma_{29}(t) + \gamma_{31}^*(t)\gamma_{31}(t) + \gamma_{31}^*(t)\gamma_{29}(t) + \gamma_{29}^*(t)\gamma_{31}(t) \right] \right\}^{1/2}. \tag{64}$$

This fidelity is shown in Figure (9).

In case of obtaining the error syndrome (1, 1), the resulting error corrected fidelity follows as

$$F(|\Psi^+\rangle, X^{[1]}\rho_q X^{[1]}) = \sqrt{\langle \Psi^+ | X^{[1]}\rho_q X^{[1]} | \Psi^+ \rangle} = \sqrt{\langle \Phi^+ | \rho_q | \Phi^+ \rangle} = \left\{ \frac{1}{2p(1,1)} \left[\sum_{k=1}^{10} \gamma_k^*(t)\gamma_k(t) + \gamma_{27}^*(t)\gamma_{27}(t) \right] \right\}^{1/2}, \quad (65)$$

which is less than 0.0035 and therefore not shown here.

After error detection by means of the syndrome (-1, 1), we obtain as fidelity

$$\begin{aligned} F(|\Psi^+\rangle, X^{[2]}Z^{[1]}\rho_q Z^{[1]}X^{[2]}) &= \sqrt{\langle \Psi^+ | X^{[2]}Z^{[1]}\rho_q Z^{[1]}X^{[2]} | \Psi^+ \rangle} = \sqrt{\langle \Phi^- | \rho_q | \Phi^- \rangle} \\ &= \left\{ \frac{1}{2p(-1,1)} \left[\gamma_{13}^*(t)\gamma_{13}(t) + \gamma_{17}^*(t)\gamma_{17}(t) + \gamma_{21}^*(t)\gamma_{21}(t) + \gamma_{25}^*(t)\gamma_{25}(t) \right] \right\}^{1/2}. \end{aligned} \quad (66)$$

It turns out to be approximately constant, very close to the value $\frac{1}{2}\sqrt{2}$.

The case with error syndrome (-1, -1) once more yields a vanishing fidelity.

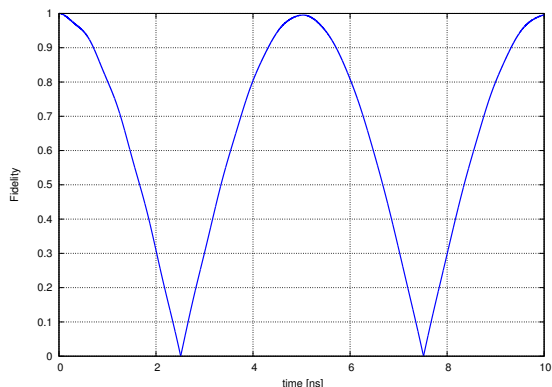


FIG. 9. Fidelity as a function of time after unitary evolution of the state $|0, 0, 0, 0\rangle|\Psi^+\rangle|\mathbf{0}, \mathbf{1}\rangle$ and subsequently obtaining error syndrome (1, -1). Parameters as in Figure (3).

V. RE-INSERTION INTO THE CIRCUIT

The stabilizer circuit has the property that re-inserting the stable state into the circuit, reproduces it. The interesting question arises how this is possibly influenced by the unitary evolution governed by the Hamiltonian before the re-insertion. We analyze this problem once more for the two stable Bell states situations for which we have already calculated the evolution. Note that we assume a certain duration of the evolution before entering the circuit again. We emphasize that this duration is arbitrary but then fixed.

A. Bell state $|\Phi^+\rangle$

In this case, we have to consider as initial state

$$|\varphi_{\text{in}}\rangle = \frac{1}{\sqrt{p(1,1)}} \sum_{k \in \bar{S}} \beta_k(t) |f_k\rangle. \quad (67)$$

In [2] and appendix B, the circuit analysis has been presented. After expressing two-qubit computational basis states in terms of the Bell states it can immediately be applied. The states of the resonators are not affected; for these we use the short-hand notation $|R_k\rangle$. We obtain as output state from the stabilizing circuit

$$\begin{aligned} |\varphi_{\text{out}}\rangle &= \frac{1}{\sqrt{2p(1,1)}} \left[\left\{ \sum_{k \in \bar{S}} \beta_k(t) |R_k\rangle \right\} \otimes |\Psi^+\rangle \otimes |\mathbf{0}, \mathbf{1}\rangle \right. \\ &\quad + \left\{ \sum_{k=0}^{10} \beta_k(t) |R_k\rangle + \beta_{27}(t) |R_{27}\rangle \right\} \otimes |\Phi^+\rangle \otimes |\mathbf{0}, \mathbf{0}\rangle \\ &\quad + \left\{ \sum_{k=0}^{10} \beta_k(t) |R_k\rangle - \beta_{27}(t) |R_{27}\rangle \right\} \otimes |\Phi^-\rangle \otimes |\mathbf{1}, \mathbf{0}\rangle \\ &\quad \left. + \left\{ \sum_{k \in \bar{S}} (-1)^k \beta_k(t) |R_k\rangle \right\} \otimes |\Psi^-\rangle \otimes |\mathbf{1}, \mathbf{1}\rangle \right], \end{aligned} \quad (68)$$

with the set $\bar{S} = \{11, 12, 15, 16, 19, 20, 23, 24\}$. Next we assume the ancillas to be measured and compute the probabilities for the various error syndromes. Recall that for the stable state, these are given by $p(1,1) = 1; p(1,-1) = p(-1,1) = p(-1,-1) = 0$. Instead of these,

we get probabilities \tilde{p} :

$$\begin{aligned}
\tilde{p}(1, 1) &= \frac{1}{2p(1, 1)} \left[\sum_{k=0}^{10} \beta_k^*(t) \beta_k(t) + \beta_{27}^*(t) \beta_{27}(t) \right. \\
&\quad \left. + \beta_0^*(t) \beta_{27}(t) + \beta_{27}^*(t) \beta_0(t) \right], \\
\tilde{p}(1, -1) &= \frac{1}{2p(1, 1)} \left[\sum_{k \in \mathcal{S}} \beta_k^*(t) \beta_k(t) + \beta_{11}^*(t) \beta_{12}(t) \right. \\
&\quad + \beta_{12}^*(t) \beta_{11}(t) + \beta_{15}^*(t) \beta_{16}(t) + \beta_{16}^*(t) \beta_{15}(t) \\
&\quad + \beta_{19}^*(t) \beta_{20}(t) + \beta_{20}^*(t) \beta_{19}(t) \\
&\quad \left. + \beta_{23}^*(t) \beta_{24}(t) + \beta_{24}^*(t) \beta_{23}(t) \right], \\
\tilde{p}(-1, 1) &= \frac{1}{2p(1, 1)} \left[\sum_{k=0}^{10} \beta_k^*(t) \beta_k(t) \right. \\
&\quad \left. + \beta_{27}^*(t) \beta_{27}(t) - \beta_0^*(t) \beta_{27}(t) - \beta_{27}^*(t) \beta_0(t) \right], \\
\tilde{p}(-1, -1) &= \frac{1}{2p(1, 1)} \left[\sum_{k \in \mathcal{S}} \beta_k^*(t) \beta_k(t) - \beta_{11}^*(t) \beta_{12}(t) \right. \\
&\quad - \beta_{12}^*(t) \beta_{11}(t) - \beta_{15}^*(t) \beta_{16}(t) - \beta_{16}^*(t) \beta_{15}(t) \\
&\quad - \beta_{19}^*(t) \beta_{20}(t) - \beta_{20}^*(t) \beta_{19}(t) \\
&\quad \left. - \beta_{23}^*(t) \beta_{24}(t) - \beta_{24}^*(t) \beta_{23}(t) \right]. \quad (69)
\end{aligned}$$

It can be readily verified that they add up to one. Comparison with (54) yields the rather intriguing result

$$\tilde{p}(1, 1) = F^2(|\Phi^+\rangle, \rho_q), \quad (70)$$

connecting the fidelity in terms of a reduced density matrix to a measurable probability. The probabilities $\tilde{p}(1, -1), \tilde{p}(-1, -1)$ are of order 10^{-9} ; consequently $p(-1, 1) \simeq 1 - p(1, 1)$.

B. Bell state $|\Psi^+\rangle$

Once more, we repeat the calculation for the Bell state $|\Psi^+\rangle$. The state after unitary evolution reads in this case

$$|\psi_{1,-1}\rangle = \frac{1}{\sqrt{p(1, -1)}} \sum_{k \in \mathcal{S}(1, -1)} \gamma_k(t) |f_k\rangle. \quad (71)$$

The input state for the stabilizer follows from re-initializing the ancillas in the ground state

$$|\psi_{\text{in}}\rangle = \frac{1}{\sqrt{p(1, -1)}} \sum_{k \in \mathcal{S}(1, -1)} \gamma_k(t) |\tilde{f}_k\rangle \otimes |\mathbf{0}, \mathbf{0}\rangle. \quad (72)$$

The next steps of the stabilizing circuit produce

$$\begin{aligned}
|\psi_{\text{out}}\rangle &= \frac{1}{\sqrt{2p(1, -1)}} \left[\left\{ \sum_{k=14,18,22,26} \gamma_k(t) |R_k\rangle \right\} \right. \\
&\quad \otimes |\Phi^+\rangle \otimes |\mathbf{0}, \mathbf{0}\rangle \\
&\quad + \left\{ \gamma_{29}(t) |R_{29}\rangle + \gamma_{31}(t) |R_{31}\rangle \right\} \otimes |\Psi^+\rangle \otimes |\mathbf{0}, \mathbf{1}\rangle \\
&\quad + \left\{ \sum_{k=14,18,22,26} \gamma_k(t) |R_k\rangle \right\} \otimes |\Phi^-\rangle \otimes |\mathbf{1}, \mathbf{0}\rangle \\
&\quad \left. + \left\{ \gamma_{31}(t) |R_{31}\rangle - \gamma_{29}(t) |R_{29}\rangle \right\} \otimes |\Psi^-\rangle \otimes |\mathbf{1}, \mathbf{1}\rangle \right]. \quad (73)
\end{aligned}$$

The corresponding probabilities follow as

$$\begin{aligned}
\tilde{p}(1, -1) &= \frac{1}{2p(1, -1)} [\gamma_{29}^*(t) \gamma_{29}(t) + \gamma_{31}^*(t) \gamma_{31}(t) \\
&\quad + \gamma_{29}^*(t) \gamma_{31}(t) + \gamma_{31}^*(t) \gamma_{29}(t)], \\
\tilde{p}(1, 1) &= \frac{1}{2p(1, -1)} \sum_{k=14,18,22,26} \gamma_k^*(t) \gamma_k(t), \\
\tilde{p}(-1, 1) &= \tilde{p}(1, 1), \\
\tilde{p}(-1, -1) &= \frac{1}{2p(1, -1)} [\gamma_{29}^*(t) \gamma_{29}(t) + \gamma_{31}^*(t) \gamma_{31}(t) \\
&\quad - \gamma_{29}^*(t) \gamma_{31}(t) - \gamma_{31}^*(t) \gamma_{29}(t)]. \quad (74)
\end{aligned}$$

As is easily checked, the sum of these probabilities equals one. Once more, we get a relation like (70)

$$\tilde{p}(1, -1) = F^2(|\Psi^+\rangle, \rho_q). \quad (75)$$

Both probabilities $p(1, -1)$ and $\tilde{p}(1, 1)$ are of order 10^{-9} . Therefore, we get $\tilde{p}(-1, -1) \simeq 1 - \tilde{p}(1, -1)$.

C. Fidelity and re-insertion

The equality of the considered re-insertion probabilities and the squares of the fidelities (70, 75) is not coincidental. We will prove and generalize this result. For the two examples of stable Bell states, we write the complete state after unitary evolution as

$$|\varphi(t)\rangle = \sum_{k=0}^{32} \mu_k(t) |f_k\rangle, \quad (76)$$

where for Bell state $|\Phi^+\rangle, \mu_k(t) = \beta_k(t)$ ($k \geq 0$) and for Bell state $|\Psi^+\rangle, \mu_0(t) = 0, \mu_k(t) = \gamma_k(t)$ ($k \geq 1$). The ancilla measurement operators for obtaining $m_{a,b} = \pm 1$, are written as

$$P_{m_a, m_b} = \mathcal{I}_{r_1} \otimes \mathcal{I}_{r_2} \otimes \mathcal{I}_{r_3} \otimes \mathcal{I}_{r_4} \otimes \mathcal{I}_{12} \otimes |\mathbf{n}_a\rangle \langle \mathbf{n}_a| \otimes |\mathbf{n}_b\rangle \langle \mathbf{n}_b|, \quad (77)$$

with $\mathbf{n}_a, \mathbf{n}_b \in \{\mathbf{0}, \mathbf{1}\}$. Recall that the measurement results (error syndromes) 1, -1 correspond respectively to the ancilla states $|\mathbf{0}\rangle, |\mathbf{1}\rangle$. Operating on the state and

subsequent normalization yields

$$P_{m_a, m_b} |\varphi(t)\rangle \rightarrow |\tilde{\varphi}(t)\rangle = \frac{1}{\sqrt{p(m_a, m_b)}} \sum_{k \in S(m_a, m_b)} \mu_k(t) |q_k\rangle |R_k\rangle \otimes |\mathbf{n}_a, \mathbf{n}_b\rangle, \quad (78)$$

with measurement probability $p(m_a, m_b)$ and data two-qubit state $|q_k\rangle$. The set $S(m_a, m_b)$ labels states corresponding with the obtained error syndrome. After this measurement, the ancillas can be amputated resulting in

$$|\tilde{\varphi}(t)\rangle = \frac{1}{\sqrt{p(m_a, m_b)}} \sum_{k \in S(m_a, m_b)} \mu_k(t) |q_k\rangle |R_k\rangle. \quad (79)$$

This state is the starting point for the computation of respective fidelities or to analyze the re-insertion into the

stabilizer circuit.

The latter starts with adding the re-initialized ancillas and use as circuit input

$$|\psi(t)\rangle = \frac{1}{\sqrt{p(m_a, m_b)}} \sum_{k \in S(m_a, m_b)} \mu_k(t) |q_k\rangle |R_k\rangle |\mathbf{0}\rangle |\mathbf{0}\rangle. \quad (80)$$

The data qubit states are expanded as

$$|q_k\rangle = \alpha_k |\Phi^+\rangle + \beta_k |\Psi^+\rangle + \gamma_k |\Phi^-\rangle + \zeta_k |\Psi^-\rangle \quad (81)$$

with normalization $|\alpha_k|^2 + |\beta_k|^2 + |\gamma_k|^2 + |\zeta_k|^2 = 1$, cf. (A.4). The allegedly ideal circuit is linear and we assume it does not affect the photon modes in the resonators. According to [2] and appendix B, its output state is then given by

$$|\Psi\rangle = \frac{1}{\sqrt{p(m_a, m_b)}} \sum_{k \in S(m_a, m_b)} \mu_k(t) |R_k\rangle \otimes (\alpha_k |\Phi^+\rangle |\mathbf{0}\rangle |\mathbf{0}\rangle + \beta_k |\Psi^+\rangle |\mathbf{0}\rangle |\mathbf{1}\rangle + \gamma_k |\Phi^-\rangle |\mathbf{1}\rangle |\mathbf{0}\rangle + \zeta_k |\Psi^-\rangle |\mathbf{1}\rangle |\mathbf{1}\rangle), \quad (82)$$

yielding the following ancilla measurement probabilities which, although not explicitly indicated, depend on m_a, m_b

$$\begin{aligned} \tilde{p}(1, 1) &= \frac{1}{p(m_a, m_b)} \sum_{k \in S(m_a, m_b)} \sum_{l \in S(m_a, m_b)} \alpha_k \alpha_l^* \mu_k(t) \mu_l^*(t) \langle R_l | R_k \rangle, \\ \tilde{p}(1, -1) &= \frac{1}{p(m_a, m_b)} \sum_{k \in S(m_a, m_b)} \sum_{l \in S(m_a, m_b)} \beta_k \beta_l^* \mu_k(t) \mu_l^*(t) \langle R_l | R_k \rangle, \\ \tilde{p}(-1, 1) &= \frac{1}{p(m_a, m_b)} \sum_{k \in S(m_a, m_b)} \sum_{l \in S(m_a, m_b)} \gamma_k \gamma_l^* \mu_k(t) \mu_l^*(t) \langle R_l | R_k \rangle, \\ \tilde{p}(-1, -1) &= \frac{1}{p(m_a, m_b)} \sum_{k \in S(m_a, m_b)} \sum_{l \in S(m_a, m_b)} \zeta_k \zeta_l^* \mu_k(t) \mu_l^*(t) \langle R_l | R_k \rangle. \end{aligned} \quad (83)$$

Note that $\langle R_l | R_k \rangle$ may also be equal to one for $k \neq l$ which lead to the earlier obtained interference terms.

The state after amputating the ancillas $|\tilde{\varphi}(t)\rangle$, cf. (79), corresponds to the density matrix

$$\tilde{\rho} = \frac{1}{p(m_a, m_b)} \sum_{k \in S(m_a, m_b)} \sum_{l \in S(m_a, m_b)} \mu_k(t) \mu_l^*(t) |q_k\rangle |R_k\rangle \langle q_l| \langle R_l|. \quad (84)$$

We explicitly introduce a complete set of resonator states as $|r_n\rangle$ and take the partial trace with respect to these degrees of freedom. In this way we obtain the two-qubit density matrix

$$\begin{aligned} \rho_q &= \frac{1}{p(m_a, m_b)} \sum_{k \in S(m_a, m_b)} \sum_{l \in S(m_a, m_b)} \sum_n \mu_k(t) \mu_l^*(t) \langle r_n | R_k \rangle \langle R_l | r_n \rangle |q_k\rangle \langle q_l|, \\ &= \frac{1}{p(m_a, m_b)} \sum_{k \in S(m_a, m_b)} \sum_{l \in S(m_a, m_b)} \mu_k(t) \mu_l^*(t) \langle R_l | R_k \rangle |q_k\rangle \langle q_l|. \end{aligned} \quad (85)$$

Using the expansion (81) yields the fidelities

$$\begin{aligned} F^2(|\Phi^+\rangle, \rho_q) &= \langle \Phi^+ | \rho_q | \Phi^+ \rangle = \tilde{p}(1, 1), \\ F^2(|\Psi^+\rangle, \rho_q) &= \langle \Psi^+ | \rho_q | \Psi^+ \rangle = \tilde{p}(1, -1), \\ F^2(|\Phi^-\rangle, \rho_q) &= \langle \Phi^- | \rho_q | \Phi^- \rangle = \tilde{p}(-1, 1), \\ F^2(|\Psi^-\rangle, \rho_q) &= \langle \Psi^- | \rho_q | \Psi^- \rangle = \tilde{p}(-1, -1). \end{aligned} \quad (86)$$

Hence we have established, for a given error syndrome m_a, m_b , identities between squared fidelities and measurement probabilities after re-insertion of the respective states into the ideal stabilizer circuit.

VI. FREE EVOLUTION & ROTATING FRAME

It may be instructive to repeat some of the computations for the noninteracting system. Of course, the free system also unitarily evolves in time. In order to partially separate consequences of free evolution a transformation to a rotating frame is useful. Formally a rotating frame transformation is equivalent to adopting the interaction representation, see e.g. [16].

A. Evolution without interaction

The Hamiltonian H_0 is obtained by setting all couplings equal to zero and corresponds to free data qubits, free ancillas and uncoupled resonators. We start with the initial state defined in eq.(15), rewritten as

$$|\varphi_0\rangle = \frac{1}{\sqrt{2}}\sqrt{2}|0, 0, 0, 0\rangle \otimes (|0, \mathbf{0}\rangle + |\mathbf{1}, \mathbf{1}\rangle) \otimes |\mathbf{0}, \mathbf{0}\rangle. \quad (87)$$

It is a superposition of the ground state and of an excited state of the ‘free’ Hamiltonian. We denote the latter by $|\tilde{E}\rangle$ with corresponding energy $\tilde{E} = E_0 + \omega'_1 + \omega'_2$. Unitary evolution governed by H_0 yields

$$|\varphi(t)\rangle = \frac{1}{\sqrt{2}}\sqrt{2}e^{-iE_0t} \left(|E_0\rangle + e^{-i\omega_+t}|\tilde{E}\rangle \right), \quad (88)$$

where $\omega_+ = \omega'_1 + \omega'_2$. It follows that measuring the ancillas gives with probability one the error syndrome $(1, 1)$. So far, so good; note the difference with the interacting case. Since there is no entanglement in this noninteracting problem, the reduced density operator still corresponds to a pure state

$$|\varphi_q(t)\rangle = \frac{1}{\sqrt{2}}\sqrt{2} (|\mathbf{0}, \mathbf{0}\rangle + e^{-i\omega_+t}|\mathbf{1}, \mathbf{1}\rangle). \quad (89)$$

Nevertheless, the obtained fidelity is oscillatory in the elapsed evolution time

$$F = |\langle\Phi^+|\varphi_q(t)\rangle| = \frac{1}{\sqrt{2}}\sqrt{2}\sqrt{1 + \cos\omega_+t}. \quad (90)$$

Our earlier results indeed coincide in the limit of vanishing couplings.

As above, we can re-insert the state after evolution (88) into the stabilizer. Changing the basis gives the following input state for fixed elapsed evolution time t :

$$|\varphi_{\text{in}}\rangle = \frac{1}{2}e^{-iE_0t}|0, 0, 0, 0\rangle \otimes \left\{ (1 + e^{-i\omega_+t})|\Phi^+\rangle + (1 - e^{-i\omega_+t})|\Phi^-\rangle \right\} \otimes |\mathbf{0}, \mathbf{0}\rangle. \quad (91)$$

The stabilizer then yields as output state

$$|\varphi_{\text{out}}\rangle = \frac{1}{2}e^{-iE_0t} \left[(1 + e^{-i\omega_+t})|0, 0, 0, 0\rangle \otimes |\Phi^+\rangle \otimes |\mathbf{0}, \mathbf{0}\rangle + (1 - e^{-i\omega_+t})|0, 0, 0, 0\rangle \otimes |\Phi^-\rangle \otimes |\mathbf{1}, \mathbf{0}\rangle \right]. \quad (92)$$

The ancilla measurement probabilities follow as

$$\begin{aligned} \tilde{p}(1, 1) &= \frac{1}{2}(1 + \cos\omega_+t), \\ \tilde{p}(-1, 1) &= \frac{1}{2}(1 - \cos\omega_+t), \\ \tilde{p}(1, -1) &= \tilde{p}(-1, -1) = 0. \end{aligned} \quad (93)$$

The sum of the probabilities is obviously one and the fidelity found in (90) satisfies

$$F^2 = \tilde{p}(1, 1). \quad (94)$$

Similar results are obtained if we start with the initial state involving the Bell state $|\Psi^+\rangle$, that is eq.(38). Unitary evolution according to H_0 leads to

$$|\psi(t)\rangle = \frac{1}{\sqrt{2}}\sqrt{2}e^{-i(E_0 + \omega'_1 + \omega_b)t}|0, 0, 0, 0\rangle \otimes \left\{ |\mathbf{1}, \mathbf{0}\rangle + e^{i\omega_-t}|\mathbf{0}, \mathbf{1}\rangle \right\} \otimes |\mathbf{0}, \mathbf{1}\rangle, \quad (95)$$

with $\omega_- = \omega'_1 - \omega'_2$. It can readily be checked that measuring the Z operators of the ancillas yields $(1, -1)$ with probability one. Recall the different results for the interacting system. The fidelity, however, again shows oscillations in the elapsed time t

$$F = |\langle\Psi^+|\varphi_q(t)\rangle| = \frac{1}{\sqrt{2}}\sqrt{2}\sqrt{1 + \cos\omega_-t}. \quad (96)$$

After re-initialization, the corresponding input state for the stabilizer is written as

$$|\psi_{\text{in}}\rangle = \frac{1}{2}e^{-i(E_0 + \omega'_1 + \omega_b)t}|0, 0, 0, 0\rangle \otimes \left\{ (1 + e^{i\omega_-t})|\Psi^+\rangle + (e^{i\omega_-t} - 1)|\Psi^-\rangle \right\} \otimes |\mathbf{0}, \mathbf{0}\rangle. \quad (97)$$

The circuit then yields as output the state

$$|\psi_{\text{out}}\rangle = \frac{1}{2}e^{-i(E_0 + \omega'_1 + \omega_b)t}|0, 0, 0, 0\rangle \otimes \left[(1 + e^{i\omega_-t})|\Psi^+\rangle \otimes |\mathbf{0}, \mathbf{1}\rangle + (e^{i\omega_-t} - 1)|\Psi^-\rangle \otimes |\mathbf{1}, \mathbf{1}\rangle \right]. \quad (98)$$

It leads to the following probabilities for the error syndromes

$$\begin{aligned} \tilde{p}(1, -1) &= \frac{1}{2}(1 + \cos\omega_-t), \\ \tilde{p}(-1, -1) &= \frac{1}{2}(1 - \cos\omega_-t), \\ \tilde{p}(1, 1) &= \tilde{p}(-1, 1) = 0. \end{aligned} \quad (99)$$

The probabilities add up to one and again the relation between the fidelity (96) and probability \tilde{p}

$$F^2 = \tilde{p}(1, -1), \quad (100)$$

is confirmed.

B. Rotating frame

1. Data qubits

The rotating frame of the two data qubits is most important. The evolution due to the Hamiltonian

$$H_0^{[12]} = H_0^{[1]} + H_0^{[2]} = -\frac{1}{2}\omega'_1\sigma_z^{[1]} - \frac{1}{2}\omega'_2\sigma_z^{[2]}, \quad (101)$$

is effectively taken into account. We explicitly perform the transformation

$$R(t) = \exp[iH_0^{[12]}t] = \exp[iH_0^{[1]}t] \exp[iH_0^{[2]}t], \quad (102)$$

where the identity holds because $[H_0^{[1]}, H_0^{[2]}] = 0$. The analysis of section III is shortly repeated for the rotating frame. To this end, we note that the introduced basis states are eigenstates of the operator $R(t)$

$$R(t)|f_k\rangle = \exp[iH_0^{[12]}t]|f_k\rangle = e^{i(\epsilon_k^{[1]} + \epsilon_k^{[2]})t}|f_k\rangle, \quad (103)$$

where $\epsilon_k^{[1]} = \pm \frac{1}{2}\omega'_1$, $\epsilon_k^{[2]} = \pm \frac{1}{2}\omega'_2$, depending on the index k . In the following we will explicitly need

$$\begin{aligned} \epsilon_0^{[1]} + \epsilon_0^{[2]} &= -\frac{1}{2}\omega_+, & \epsilon_{27}^{[1]} + \epsilon_{27}^{[2]} &= \frac{1}{2}\omega_+, \\ \epsilon_{29}^{[1]} + \epsilon_{29}^{[2]} &= \frac{1}{2}\omega_-, & \epsilon_{31}^{[1]} + \epsilon_{31}^{[2]} &= -\frac{1}{2}\omega_-. \end{aligned} \quad (104)$$

It is also convenient to define the modified functions

$$\tilde{\beta}_k(t) = e^{i(\epsilon_k^{[1]} + \epsilon_k^{[2]})t}\beta_k(t), \quad \tilde{\gamma}_k(t) = e^{i(\epsilon_k^{[1]} + \epsilon_k^{[2]})t}\gamma_k(t). \quad (105)$$

Now we proceed to the evolution of two previously analyzed Bell states.

a. Bell state $|\Phi^+\rangle$

The evolved state (17) in the rotated frame is given by

$$|\phi_R(t)\rangle = R(t)|\phi(t)\rangle = \sum_{k=0}^{32} \tilde{\beta}_k(t)|f_k\rangle. \quad (106)$$

Since $\tilde{\beta}(t)\tilde{\beta}^*(t) = \beta(t)\beta^*(t)$, the measurement probabilities of obtaining the various error syndromes do not

change. The density matrix (52) corresponding to the syndrome (1, 1), however, does change:

$$\rho^R = \frac{1}{p(1,1)} \sum_{k \in \bar{S}} \sum_{l \in \bar{S}} \tilde{\beta}_k(t)\tilde{\beta}_l^*(t)|\tilde{f}_k\rangle\langle\tilde{f}_l|. \quad (107)$$

As a consequence, the fidelity (54) is also modified

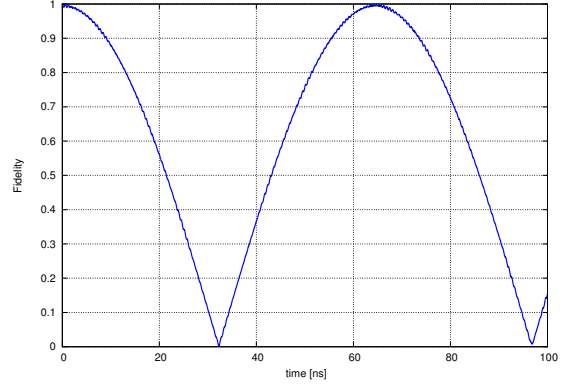


FIG. 10. Fidelity in the rotating frame as a function of time after unitary evolution of the state $|0,0,0,0\rangle|\Phi^+\rangle|0,0\rangle$ and subsequently obtaining error syndrome (1, 1). Parameters as in Figure (3). Compare to Figure (7).

$$\begin{aligned} F_R(|\Phi^+\rangle, \rho_q^R) &= \sqrt{\langle\Phi^+|\rho_q^R|\Phi^+\rangle} \\ &= \left\{ \frac{1}{2p(1,1)} \left[\sum_{k=0}^{10} \beta_k^*(t)\beta_k(t) + \beta_{27}^*(t)\beta_{27}(t) + \tilde{\beta}_0^*(t)\tilde{\beta}_{27}(t) + \tilde{\beta}_{27}^*(t)\tilde{\beta}_0(t) \right] \right\}^{1/2} \\ &= \left\{ \frac{1}{2p(1,1)} \left[\sum_{k=0}^{10} \beta_k^*(t)\beta_k(t) + \beta_{27}^*(t)\beta_{27}(t) + e^{i\omega_+t}\beta_0^*(t)\beta_{27}(t) + e^{-i\omega_+t}\beta_{27}^*(t)\beta_0(t) \right] \right\}^{1/2}, \end{aligned} \quad (108)$$

as shown in Figure (10). It is readily verified that the relation between probability for finding result (1, 1) after re-insertion into the stabilizer and fidelity (70) is also valid in the rotating frame:

$$\tilde{p}_R(1,1) = F^2(|\Phi^+\rangle, \rho_q^R). \quad (109)$$

Analogous computations for the error syndrome (1, -1) yield a modification of the fidelity (61) as well

$$\begin{aligned} F_R(|\Phi^+\rangle, X^{[2]}\rho_q^R X^{[2]}) &= \sqrt{\langle\Phi^+|X^{[2]}\rho_q^R X^{[2]}|\Phi^+\rangle} = \sqrt{\langle\Psi^+|\rho_q|\Psi^+\rangle} \\ &= \left\{ \frac{1}{2p(1,-1)} \left[\beta_{29}^*(t)\beta_{29}(t) + \beta_{31}^*(t)\beta_{31}(t) + \tilde{\beta}_{31}^*(t)\tilde{\beta}_{29}(t) + \tilde{\beta}_{29}^*(t)\tilde{\beta}_{31}(t) \right] \right\}^{1/2} \\ &= \left\{ \frac{1}{2p(1,-1)} \left[\beta_{29}^*(t)\beta_{29}(t) + \beta_{31}^*(t)\beta_{31}(t) + e^{i\omega_-t}\beta_{31}^*(t)\beta_{29}(t) + e^{-i\omega_-t}\beta_{29}^*(t)\beta_{31}(t) \right] \right\}^{1/2}. \end{aligned} \quad (110)$$

This result is depicted in Figure (11). The final fidelities after having obtained the error syndromes $(-1, 1)$ and $(-1, -1)$ do not change in the rotating frame. The reason is that these expressions do not contain interference between $\beta_k(t)$ functions with different indices k .

b. Bell state $|\Psi^+\rangle$

The unitarily evolved state corresponding to the two qubit Bell state $|\Psi^+\rangle$ reads in the rotating frame

$$|\psi_R(t)\rangle = R(t)|\psi(t)\rangle = \sum_{k=1}^{32} \tilde{\gamma}_k(t)|f_k\rangle. \quad (111)$$

The measurement probabilities once more do not change because $\tilde{\gamma}(t)\tilde{\gamma}^*(t) = \gamma(t)\gamma^*(t)$. The density matrix resulting from the error syndrome $(1, -1)$ has two interference terms and, as a consequence, it gets modified. Concomitantly, we obtain a modification of the fidelity (64):

$$\begin{aligned} F_R(|\Psi^+\rangle, \rho_q^R) &= \sqrt{\langle \Psi^+ | \rho_q^R | \Psi^+ \rangle} \\ &= \sqrt{\frac{1}{2p(1, -1)} \left[\gamma_{29}^*(t)\gamma_{29}(t) + \gamma_{31}^*(t)\gamma_{31}(t) + \tilde{\gamma}_{31}^*(t)\tilde{\gamma}_{29}(t) + \tilde{\gamma}_{29}^*(t)\tilde{\gamma}_{31}(t) \right]} \\ &= \sqrt{\frac{1}{2p(1, -1)} \left[\gamma_{29}^*(t)\gamma_{29}(t) + \gamma_{31}^*(t)\gamma_{31}(t) + e^{i\omega_- t}\gamma_{31}^*(t)\gamma_{29}(t) + e^{-i\omega_- t}\gamma_{29}^*(t)\gamma_{31}(t) \right]}. \end{aligned} \quad (112)$$

This result is shown in Figure (12). The relation between probability after re-insertion and fidelity is once again valid

$$\tilde{p}_R(1, -1) = F^2(|\Psi^+\rangle, \rho_q^R). \quad (113)$$

The other fidelities do not contain interference terms and are therefore not changed in the rotating frame.

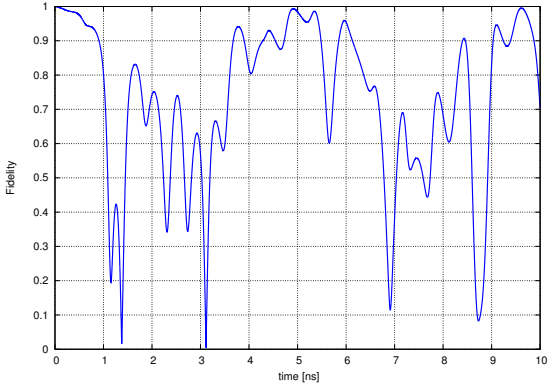


FIG. 11. Fidelity in the rotating frame as a function of time after unitary evolution of the state $|0, 0, 0, 0\rangle|\Phi^+\rangle|\mathbf{0}, \mathbf{0}\rangle$, subsequently obtaining error syndrome $(1, -1)$ and error correction. Parameters as in Figure (3). Compare to Figure (8).

2. Including ancillas

It is straightforward to extend the rotating frame with the ancillas. Their ‘free’ Hamiltonians commute and they also commute with $H_0^{[12]}$. If we denote the extended operator as \mathcal{R} , we obtain

$$\mathcal{R}(t)|f_k\rangle = e^{i(\epsilon_k^{[1]} + \epsilon_k^{[2]} + \epsilon_k^{[a]} + \epsilon_k^{[b]})t}|f_k\rangle, \quad (114)$$

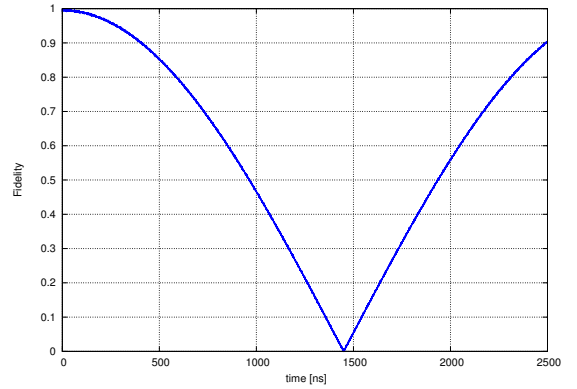


FIG. 12. Fidelity in the rotating frame as a function of time after unitary evolution of the state $|0, 0, 0, 0\rangle|\Psi^+\rangle|\mathbf{0}, \mathbf{0}\rangle$ and subsequently obtaining error syndrome result $(1, -1)$. Parameters as in Figure (3). Compare to Figure (9).

with $\epsilon_k^{[a]} = \pm \frac{1}{2}\omega_a, \epsilon_k^{[b]} = \pm \frac{1}{2}\omega_b$, once more depending on the index k . The relevant energies are given by

$$\begin{aligned} \epsilon_0^{[1]} + \epsilon_0^{[2]} &= -\frac{1}{2}\omega_+ - \frac{1}{2}\omega_a - \frac{1}{2}\omega_b, \\ \epsilon_{27}^{[1]} + \epsilon_{27}^{[2]} &= \frac{1}{2}\omega_- - \frac{1}{2}\omega_a - \frac{1}{2}\omega_b, \\ \epsilon_{29}^{[1]} + \epsilon_{29}^{[2]} &= \frac{1}{2}\omega_- - \frac{1}{2}\omega_a + \frac{1}{2}\omega_b, \\ \epsilon_{31}^{[1]} + \epsilon_{31}^{[2]} &= -\frac{1}{2}\omega_- - \frac{1}{2}\omega_a + \frac{1}{2}\omega_b. \end{aligned} \quad (115)$$

The functions $\beta_k(t)$ and $\gamma_k(t)$ are now modified as

$$\begin{aligned} \hat{\beta}_k(t) &= e^{i(\epsilon_k^{[1]} + \epsilon_k^{[2]} + \epsilon_k^{[a]} + \epsilon_k^{[b]})t}\beta_k(t), \\ \hat{\gamma}_k(t) &= e^{i(\epsilon_k^{[1]} + \epsilon_k^{[2]} + \epsilon_k^{[a]} + \epsilon_k^{[b]})t}\gamma_k(t). \end{aligned} \quad (116)$$

The calculation now proceeds as above but now with the functions $\hat{\beta}_k(t)$ and $\hat{\gamma}_k(t)$. The new phase factors due to the ancillas, however, cancel in the terms which could have altered the previous results for the fidelities. As a

consequence, the obtained fidelities do *not* change in this extended rotated frame.

VII. THEORETICAL DISCUSSION

A. Error analysis

The stabilizing circuit with two ancilla qubits and two data qubits is a building block in surface codes for error correction [2–4]. Of course, this has motivated our choice for these investigations. The circuit, including the ancilla measurement and possibly error correction can deal with errors on the data qubits which occur before performing the circuit. The unitary evolution we have analyzed is supposed to take place between the circuit unitary operations and ancilla measurements. Even if one would be able to interpret the consequences as ‘errors’, it is shown that they cannot be corrected in the usual way, that is applying the usual transformation on the data qubits based on the error syndromes.

With respect to the interpretation as ‘errors’, there is no obvious identification of the error type. In [1] coherent gate errors, environmental decoherence, initialization and measurement errors as well as loss and leakage are discussed. One may consider the electromagnetic resonators and even the ancillas as ‘environment’; the ancillas are measured, the remaining resonators are traced out. It will be further analyzed below using the concept of quantum operations [14, 17]. At this point, we can already state that it does not yield a satisfactory correction mechanism. Our findings are more similar to those in [12], where a gate-error analysis for transmon qubits is presented. The unitary evolution of the total system is also calculated in that study. As in our case, it is inherently unitary but yields detrimental effects on gates in the computational subspace. The ‘errors’ are also systematic but appear incoherent in that subspace. In both analyses, they originate from entanglement with other states due to Hamiltonian evolution; in [12] noncomputational transmon states and the resonator – in our work, ancillas and resonators.

Although no quantum code for the stabilizing circuit is developed as such, there is a certain resemblance because of the use of certain subspaces in a larger Hilbert space. Quantum error correction by means of coding, e.g. Shor’s nine-bit code, is for instance explained in [17]. Within a complete Hilbert space a code subspace is defined. The considered error operators map the code subspace to orthogonal subspaces. Errors can then be detected, distinguished and eventually corrected by determining in which subspace the system is. It can be done without disturbance and destroying the coherence; superposition and entanglement are essential in the process. Returning to the stabilizing circuit, we recall that a product state of a general two-data qubit state and the ancillas in the ground state is put in. The initial subspace is therefore four-dimensional, whereas the com-

plete qubit Hilbert space is sixteen-dimensional. After the defined operations, the final state also belongs to a four-dimensional subspace, having the specific structure given in appendix B. The ancilla measurements subsequently project to one of the one-dimensional subspaces of the data qubit Hilbert space. However, if the final state evolves unitarily according to the system Hamiltonian then the four-dimensional subspace is abandoned. It explains why this particular error identification and correction does not work. Assume that the initial state is one of the Bell states. Without evolution the corresponding probabilities for the measurement outcomes are zero or one. This is no longer true after unitary evolution. Two more aspects are important. First, even if the ancilla measurement indicates no error, the final data qubit state is not the expected one. Secondly, if the syndrome indicates an error, the usual error correction transformations, cf. section II B, do not work. Note that these findings do not depend merely on the inclusion of the resonators as degrees of freedom. Indeed, in a model with only spin-exchange interaction between adjacent qubits, similar results have been obtained [18]. Of course, in the model with resonators one has to extend the ideal qubit state with resonators; here we have taken a product state with empty resonators. There remains a noticeable difference in the results compared to the spin model. Since a final data qubit state has to be identified the resonators have to be traced out after the evolution; it does not matter whether this is done before or after the measurement, see VII C. In any case, the final data qubit ‘state’ is not a pure state –as in the exchange model– but can only be described by means of a density operator. In both models, however, the essential phenomenon is that the evolution operator leads the state out of the stable subspace.

B. Stabilizers in the Heisenberg picture

The concept of the X, Z stabilizing circuit has also been demonstrated by calculating with stabilizers instead of states [2]. To this end, the Heisenberg representation is used. In particular, it is necessary to perform CNOT operations on products of the X, Z and \mathcal{I} operators. Here we do not reproduce the derivation of appendix B of [2], but only note that the resulting two stabilizers are $X^{[a]}X^{[1]}X^{[2]}\mathcal{I}^{[b]}$ and $\mathcal{I}^{[a]}Z^{[1]}Z^{[2]}Z^{[b]}$. These operators commute and ancilla measurements indeed yield the two-qubit stabilizers $Z^{[1]}Z^{[2]}$ and $X^{[1]}X^{[2]}$. However, in case of unitary evolution before the measurement we need to evolve the four-qubit stabilizers since we are in the Heisenberg representation. Without doing the explicit calculation, it is easily seen that the two stabilizers are not invariant under time-evolution. Recalling that in the Heisenberg equation for an operator A the commutator $[A, H]$ drives non-trivial evolution, the commutators of the two four-qubit stabilizers with the full Hamiltonian are to be calculated. Here we only note that these commutators are nonzero causing the stabilizers to change.

Equivalently, this can be seen using the explicitly constructed evolution operator $U(t)$ to find the evolution $A(t) = U(t)AU^\dagger(t)$. Once again, without doing the computation completely, it is clear that the stabilizers evolve non-trivially. As a consequence, the stabilizing mechanism will fail after finite time t . Resonator operators will appear in the evolution of the stabilizers. After the evolution time t they need to be traced out gain. The latter does of course not apply to the interacting spin system [18]. Nevertheless, the stabilizers also evolve in time, reflecting the degradation of the stabilizer formalism taking into account full Hamiltonian evolution.

In larger systems on which a surface code can be implemented similar observations hold. Consider, for example, Surface 17 [5], which contains the studied two data qubits, two ancillas system as subsystems. Surface 17 consists out of nine data qubits and eight ancillas. In this system, eight stabilizers can be identified [2]. These constrain the 2^9 -dimensional data qubit space to a large extent. However, a two-dimensional subspace is not constrained. It can be exploited as computational space spanned by two logical qubits $|\mathbf{0}_L\rangle, |\mathbf{1}_L\rangle$. Concomitantly, logical operators Z_L, X_L can be defined. Our concerns based on unitary evolution describing the complete dynamics apply here as well. Stabilizers and logical operators evolve in time and the associated subspaces are not invariant. Recently, a numerical study testing quantum fault tolerance on small systems has appeared [13].

C. Quantum operations

The framework of quantum operations has been developed to deal with quantum noise by means of error correction [14, 17]. The eventual error correction is typically done for the code subspace which, of course, is defined for a specific code. For example the three qubit bit flip code uses the two-dimensional code subspace spanned by the states $|000\rangle$ and $|111\rangle$. The formalism aims at taking into account the interaction of the system of interest and the environment. It includes selective dynamics, where the environment is not observed, as well as nonselective dynamics, where a measurement on the environment is made. Various approaches for formulating quantum operations are presented in [14].

Here we use quantum operations to describe the processes in our system. Note that we do not consider a quantum code and, consequently, there is no code subspace. Noise is not considered and, concomitantly, there is no actual environment. We may, however, consider or rather describe the electromagnetic resonators as environment since we eventually focus on the qubits by taking the partial trace with respect to these degrees of freedom. Because the resonators are not measured, this dynamics is nonselective. In addition, the ancillas can be considered as environment as well. The reason is that they are measured also implying that their dynamics is selective. We will see below that the order of tracing out resonators

and measuring the ancillas is not relevant.

Quantum operations are defined as operators transforming density matrices. For the full system we merely use the symbol ρ , for data qubits ρ_q , for ancillas ρ_a and for resonators ρ_r . The ideal circuit has the transformation property

$$|b_m\rangle|\mathbf{0}, \mathbf{0}\rangle\langle b_m|\langle\mathbf{0}, \mathbf{0}| \longrightarrow |b_m\rangle|a_m\rangle\langle a_m|\langle b_m|, \quad (117)$$

where $|b_m\rangle, m \in \{1, 2, 3, 4\}$ denotes one of the Bell states with corresponding ancilla state $|a_m\rangle$. Next we extend this matrix with empty resonators thereby defining the initial density matrix before unitary evolution

$$\begin{aligned} \rho(0) &= |0, 0, 0, 0\rangle|b_m\rangle|a_m\rangle\langle a_m|\langle b_m|\langle 0, 0, 0, 0| \\ &= \rho_r(0) \otimes \rho_q(0) \otimes \rho_a(0). \end{aligned} \quad (118)$$

Unitary evolution yields the density matrix

$$\rho(t) = U(t) (\rho_r(0) \otimes \rho_q(0) \otimes \rho_a(0)) U^\dagger(t). \quad (119)$$

Note that we explicitly have constructed the evolution operator up to (and including) the second excitation level. Measuring the ancillas is described by the operators P_k where $k = (1, 1) \dots (-1, -1)$ labels the measurement result, *i.e.*, the error syndrome. The subsequent ‘amputation’ of the projected ancilla state can formally be done via a partial trace. Finally we trace out the resonators to obtain the quantum operation

$$\begin{aligned} \rho_q(0) \rightarrow \rho_q(t) &= \mathcal{E}(\rho_q) \\ &= \text{tr}_r \left[\text{tr}_a \left[P_k U(t) (\rho_r(0) \otimes \rho_q(0) \otimes \rho_a(0)) U^\dagger P_k \right] \right]. \end{aligned} \quad (120)$$

Alternatively, we take the partial trace with respect to the resonators before the measurement

$$\begin{aligned} \tilde{\rho}_q(0) \rightarrow \tilde{\rho}_q(t) &= \tilde{\mathcal{E}}(\rho_q) \\ &= \text{tr}_a \left[P_k \text{tr}_r \left[U(t) (\rho_r(0) \otimes \rho_q(0) \otimes \rho_a(0)) U^\dagger \right] P_k \right]. \end{aligned} \quad (121)$$

Inserting the initial density matrix yields

$$\mathcal{E}(\rho_q) = \tilde{\mathcal{E}}(\rho_q) = \sum_r A_{kr} \rho_q A_{kr}^\dagger, \quad (122)$$

with the data qubit operators

$$A_{kr} = \langle r a_k | U(t) | r_0 a_m \rangle. \quad (123)$$

The resonator states are here denoted by $|r\rangle$ and $|r_0\rangle = |0, 0, 0, 0\rangle$. The result generalizes the simplest operator-sum representation [14], because of the additional trace over the resonators. Its normalized form is given by

$$\mathcal{E}(\rho_q) = \frac{\sum_r A_{kr} \rho_q A_{kr}^\dagger}{\text{tr} \left[\sum_r A_{kr} \rho_q A_{kr}^\dagger \right]}, \quad (124)$$

where the normalization equals the probability that the measurement outcome labelled k is obtained for the defined initial Bell state. The operators A , often denoted by E , are called operational elements in [14]; in our case

they depend on the evolution time. The theory of quantum error correction exploits these operators to derive conditions for error correction on a subspace defined by a certain quantum code [14]. Note that in our case error correction would mean reversing the unitary evolution for the data qubits. Since this appears to be unfeasible in practice, we do not pursue this.

We conclude this section by noting that we have already derived explicit expressions for the quantum operations (124). For the initial Bell state $|\Phi^+\rangle$ they are given in (53), (56), (60) and (62). The trivial, *i.e.*, time-independent pure computational basis state, result (62) can be easily ‘corrected’ because

$$C_N \left(\mathbf{H}^{[1]} \otimes \mathcal{I}^{[2]} \right) |\mathbf{0}, \mathbf{0}\rangle = |\Phi^+\rangle, \quad (125)$$

where \mathbf{H} is the Hadamard transformation and C_N denotes the CNOT operation.

D. Synopsis

At this point, it may be useful to summarize the results of our study. First, we have computed unitary evolutions of the extended output states of the stabilized circuit. The extension is to include the empty resonators. For free evolution, *i.e.*, zero couplings, the error syndrome indicating no error is obtained with certainty. This does not longer hold for the interacting case, where these probabilities become somewhat smaller than one. Concomitantly, the probabilities for a different syndrome which indicates an error are nonzero. The measurement operator for the error syndrome indicating no error does in general *not* project the evolved state on the desired target two-qubit resonator state. The exception is the case where the initial state is an eigenstate of the Hamiltonian which governs the time evolution. There are two related consequences. Calculating the fidelity of the two-qubit subsystem with the target Bell states, which is done by taking the partial trace of the resonator degrees of freedom, yields oscillating fidelities with high frequencies. Secondly, re-inserting the evolved two-qubit resonator stated completed with (possibly) re-initialized ancillas in the ground state, does not lead to the desired target state. The concomitant measurement probabilities resonate once again with high frequencies.

Similar results follow for error-corrected two-qubit states constructed after the first error detection. Neither high fidelities nor subsequent desired measurement probabilities close to one are obtained. It happens for free as well as complete, that is including the interactions, evolution. In other words, Hamiltonian governed unitary evolution causes problems for the stabilizing circuit as the target states are no energy eigenstates. For free evolution, however, target states are linear superpositions of eigenstates and, as a consequence, the probability of getting the syndrome indicating no error remains one. In the interacting case, even the latter breaks down although the mentioned probability is close to one whereas

the error detection probabilities are rather small. Another difference for nonzero coupling is the fact that the two-qubit subsystem can only be described with a density matrix which does *not* correspond to a pure state. This is a consequence of the entanglement of data qubits and the resonators, even after the measurement of the ancillas. For the noninteracting system, the two-qubit resonator system is described by a product state and taking the partial trace yields a density matrix which describes a pure state. In fact, the results for H_0 can be obtained without invoking the density matrix formalism.

The calculations have also been done in the rotating frame of the data qubits. Measurement probabilities for the various error syndromes are not altered. The fidelities, however, do change. The observed time variations are slower, which indicates the expected cancellation of the highest frequency components. Nevertheless, with one exception, the resulting fidelities decrease rather fast. Extending the rotating frame with respect to the ancillas does not change the results.

VIII. CONCLUSION

Our semi-analytical analysis of the X and Z stabilizing circuit has revealed deteriorating consequences of unitary evolution of the complete, *i.e.*, qubits and resonators, interacting system. Probabilities for error syndromes indicating no error, therefore ideally equal one, decrease to the range 0.992 – 0.999. Fidelities of the augmented density matrices and the stable target state, also ideally one, oscillate between 0 and 1. After having obtained an error syndrome indicating an error, the usual error correction does not apply. The latter is *a fortiori* explained because unitary evolution does lead out of subspaces on which the usual error correction does work. The explanation in terms of the stabilizers of the circuits is that they are no longer conserved, *i.e.*, evolve non-trivially governed by the complete Hamiltonian.

Several caveats should be kept in mind with respect to this research. We have only addressed part of the effects of unitary evolution, that is only in a time interval between the last unitary operation in the stabilizing circuit and the ancilla measurement. The latter is supposed to be perfect. It is also assumed that the circuit performs perfectly. The rotating wave approximation has been made in the interaction terms. Environmental decoherence is neglected. Only the four-qubit system has been considered, etc.

Nevertheless, we think that the results can be relevant for the further development of quantum error correction and fault-tolerant computation. Recall that these concepts rely on the applicability of some mathematical error model, like one-qubit Pauli channels [14]. The latter cannot describe the deleterious effects on the computational subspace we have identified. The preliminary, somewhat discomfoting, overall conclusion is that the existing stabilizer codes are not sufficient to handle the

consequences of unitary evolution of coupled (transmon-like) qubit–resonator quantum systems.

ACKNOWLEDGMENTS

The authors thank B.M. Terhal and B. Criger for stimulating discussions. This research is supported by the Early Research Programme of the Netherlands Organisation for Applied Scientific Research (TNO). Additional support from the Top Sector High Tech Systems and Materials is highly appreciated.

Appendix A: Definitions and notation

Throughout this paper we adopt units with $\hbar = 1$.

For the two data qubit system we use the following definition of the Bell states

$$\begin{aligned} |\Phi^\pm\rangle &= \frac{1}{\sqrt{2}}\sqrt{2}(|\mathbf{0}, \mathbf{0}\rangle \pm |\mathbf{1}, \mathbf{1}\rangle), \\ |\Psi^\pm\rangle &= \frac{1}{\sqrt{2}}\sqrt{2}(|\mathbf{0}, \mathbf{1}\rangle \pm |\mathbf{1}, \mathbf{0}\rangle). \end{aligned} \quad (\text{A.1})$$

The operators $\sigma_z^{[1]}, \sigma_z^{[2]}, \sigma_x^{[1]}$ and $\sigma_x^{[2]}$ are also respectively

denoted by $Z^{[1]}, Z^{[2]}, X^{[1]}, X^{[2]}$. The superindex refers to the qubit; for the ancillas the indices a, b will be analogously used. Below we need the action of the X -operators on the basis states

$$\begin{aligned} X^{[1]}|\Phi^+\rangle &= |\Psi^+\rangle, & X^{[2]}|\Phi^+\rangle &= |\Psi^+\rangle, \\ X^{[1]}|\Phi^-\rangle &= -|\Psi^-\rangle, & X^{[2]}|\Phi^-\rangle &= |\Psi^-\rangle, \\ X^{[1]}|\Psi^+\rangle &= |\Phi^+\rangle, & X^{[2]}|\Psi^+\rangle &= |\Phi^+\rangle, \\ X^{[1]}|\Psi^-\rangle &= -|\Phi^-\rangle, & X^{[2]}|\Psi^-\rangle &= |\Phi^-\rangle. \end{aligned} \quad (\text{A.2})$$

Because we will consider a X and Z stabilizer circuit, we apply the Z -operators to the Bell states as well and get

$$\begin{aligned} Z^{[1]}|\Phi^+\rangle &= |\Phi^-\rangle, & Z^{[2]}|\Phi^+\rangle &= |\Phi^-\rangle, \\ Z^{[1]}|\Phi^-\rangle &= |\Phi^+\rangle, & Z^{[2]}|\Phi^-\rangle &= |\Phi^+\rangle, \\ Z^{[1]}|\Psi^+\rangle &= |\Psi^-\rangle, & Z^{[2]}|\Psi^+\rangle &= -|\Psi^-\rangle, \\ Z^{[1]}|\Psi^-\rangle &= |\Psi^+\rangle, & Z^{[2]}|\Psi^-\rangle &= -|\Psi^+\rangle. \end{aligned} \quad (\text{A.3})$$

A general two-qubit state, usually written as superposition of computational states, can also be written as a linear combination of the Bell states, *i.e.*,

$$|\Psi_{12}\rangle = A_+|\Phi^+\rangle + A_-|\Phi^-\rangle + B_+|\Psi^+\rangle + B_-|\Psi^-\rangle, \quad (\text{A.4})$$

with $|A_+|^2 + |A_-|^2 + |B_+|^2 + |B_-|^2 = 1$.

Appendix B: Circuit analysis in terms of Bell states

In this appendix we also use the one-qubit states

$$|\pm\rangle = \frac{1}{\sqrt{2}}\sqrt{2}(|\mathbf{0}\rangle \pm |\mathbf{1}\rangle). \quad (\text{B.1})$$

Recall that they are obtained via the Hadamard transformation on the computational states

$$\mathbf{H}|\mathbf{0}\rangle = |+\rangle, \quad \mathbf{H}|\mathbf{1}\rangle = |-\rangle. \quad (\text{B.2})$$

We re-analyze the X and Z stabilizing circuit in terms of Bell states, cf. [2]. Explicitly the following steps are done:

1. Initialize both ancillas in their ground state. The data qubits are in a general state given in (A.4). Consequently the initial four-qubit state reads

$$|\psi_1\rangle = |\mathbf{0}\rangle (A_+|\Phi^+\rangle + A_-|\Phi^-\rangle + B_+|\Psi^+\rangle + B_-|\Psi^-\rangle) |\mathbf{0}\rangle. \quad (\text{B.3})$$

2. Perform a Hadamard operation on ancilla A

$$|\psi_2\rangle = |+\rangle (A_+|\Phi^+\rangle + A_-|\Phi^-\rangle + B_+|\Psi^+\rangle + B_-|\Psi^-\rangle) |\mathbf{0}\rangle. \quad (\text{B.4})$$

3. With ancilla A as control and qubit 1 as target, a CNOT is applied:

$$\begin{aligned} |\psi_3\rangle &= \frac{1}{\sqrt{2}}\sqrt{2}[|\mathbf{0}\rangle (A_+|\Phi^+\rangle + A_-|\Phi^-\rangle + B_+|\Psi^+\rangle + B_-|\Psi^-\rangle) \\ &\quad + |\mathbf{1}\rangle (A_+|\Psi^+\rangle - A_-|\Psi^-\rangle + B_+|\Phi^+\rangle - B_-|\Phi^-\rangle)] |\mathbf{0}\rangle. \end{aligned} \quad (\text{B.5})$$

4. A second CNOT is applied, again with ancilla A as control. Qubit 2, however, is the target:

$$\begin{aligned} |\psi_4\rangle &= \frac{1}{\sqrt{2}}\sqrt{2}[|\mathbf{0}\rangle (A_+|\Phi^+\rangle + A_-|\Phi^-\rangle + B_+|\Psi^+\rangle + B_-|\Psi^-\rangle) \\ &\quad + |\mathbf{1}\rangle (A_+|\Phi^+\rangle - A_-|\Phi^-\rangle + B_+|\Psi^+\rangle - B_-|\Psi^-\rangle)] |\mathbf{0}\rangle \\ &= |+\rangle (A_+|\Phi^+\rangle + B_+|\Psi^+\rangle) |\mathbf{0}\rangle + |-\rangle (A_-|\Phi^-\rangle + B_-|\Psi^-\rangle) |\mathbf{0}\rangle. \end{aligned} \quad (\text{B.6})$$

5. A CNOT is applied with data qubit 1 as control and ancilla B as target. We omit the intermediate result $|\psi_5\rangle$ because it is more convenient to combine this operation with the next step.
6. A CNOT is applied with data qubit 2 as control and ancilla B as target. The two CNOTs yield for the relevant states

$$|\Phi^\pm\rangle|\mathbf{0}\rangle \rightarrow |\Phi^\pm\rangle|\mathbf{0}\rangle, \quad |\Psi^\pm\rangle|\mathbf{0}\rangle \rightarrow |\Psi^\pm\rangle|\mathbf{1}\rangle. \quad (\text{B.7})$$

Therefore, the resulting four-qubit state reads

$$|\psi_6\rangle = A_+|+\rangle|\Phi^+\rangle|\mathbf{0}\rangle + B_+|+\rangle|\Psi^+\rangle|\mathbf{1}\rangle + A_-|-\rangle|\Phi^-\rangle|\mathbf{0}\rangle + B_-|-\rangle|\Psi^-\rangle|\mathbf{1}\rangle. \quad (\text{B.8})$$

7. A Hadamard is performed on ancilla A; we obtain

$$|\psi_7\rangle = A_+|\mathbf{0}\rangle|\Phi^+\rangle|\mathbf{0}\rangle + B_+|\mathbf{0}\rangle|\Psi^+\rangle|\mathbf{1}\rangle + A_-|\mathbf{1}\rangle|\Phi^-\rangle|\mathbf{0}\rangle + B_-|\mathbf{1}\rangle|\Psi^-\rangle|\mathbf{1}\rangle. \quad (\text{B.9})$$

8. Both ancillas are eventually measured in their standard basis. The concomitant measurement operators are given by

$$\begin{aligned} P_{11} &= |\mathbf{0}\rangle\langle\mathbf{0}| \otimes \mathcal{I}_{12} \otimes |\mathbf{0}\rangle\langle\mathbf{0}|, & P_{-11} &= |\mathbf{1}\rangle\langle\mathbf{1}| \otimes \mathcal{I}_{12} \otimes |\mathbf{0}\rangle\langle\mathbf{0}|, \\ P_{1-1} &= |\mathbf{0}\rangle\langle\mathbf{0}| \otimes \mathcal{I}_{12} \otimes |\mathbf{1}\rangle\langle\mathbf{1}|, & P_{-1-1} &= |\mathbf{1}\rangle\langle\mathbf{1}| \otimes \mathcal{I}_{12} \otimes |\mathbf{1}\rangle\langle\mathbf{1}|, \end{aligned} \quad (\text{B.10})$$

with probabilities for the outcomes $\pm 1, \pm 1$

$$\begin{aligned} p(1, 1) &= |A_+|^2, & p(1, -1) &= |B_+|^2, \\ p(-1, 1) &= |A_-|^2, & p(-1, -1) &= |B_-|^2. \end{aligned} \quad (\text{B.11})$$

The corresponding final two-qubit states are the Bell states

$$\begin{aligned} \text{syndrome}(1, 1) &: |\Phi^+\rangle, & \text{syndrome}(1, -1) &: |\Psi^+\rangle, \\ \text{syndrome}(-1, 1) &: |\Phi^-\rangle, & \text{syndrome}(-1, -1) &: |\Psi^-\rangle. \end{aligned} \quad (\text{B.12})$$

Appendix C: Basis states and matrix elements

1. First excitation level

In this subspace, we choose the basis states

$$\begin{aligned} |e_1\rangle &= |1, 0, 0, 0\rangle \otimes |\mathbf{0}, \mathbf{0}\rangle \otimes |\mathbf{0}, \mathbf{0}\rangle, & |e_2\rangle &= |0, 1, 0, 0\rangle \otimes |\mathbf{0}, \mathbf{0}\rangle \otimes |\mathbf{0}, \mathbf{0}\rangle, \\ |e_3\rangle &= |0, 0, 1, 0\rangle \otimes |\mathbf{0}, \mathbf{0}\rangle \otimes |\mathbf{0}, \mathbf{0}\rangle, & |e_4\rangle &= |0, 0, 0, 1\rangle \otimes |\mathbf{0}, \mathbf{0}\rangle \otimes |\mathbf{0}, \mathbf{0}\rangle, \\ |e_5\rangle &= |0, 0, 0, 0\rangle \otimes |\mathbf{1}, \mathbf{0}\rangle \otimes |\mathbf{0}, \mathbf{0}\rangle, & |e_6\rangle &= |0, 0, 0, 0\rangle \otimes |\mathbf{0}, \mathbf{1}\rangle \otimes |\mathbf{0}, \mathbf{0}\rangle, \\ |e_7\rangle &= |0, 0, 0, 0\rangle \otimes |\mathbf{0}, \mathbf{0}\rangle \otimes |\mathbf{1}, \mathbf{0}\rangle, & |e_8\rangle &= |0, 0, 0, 0\rangle \otimes |\mathbf{0}, \mathbf{0}\rangle \otimes |\mathbf{0}, \mathbf{1}\rangle. \end{aligned} \quad (\text{C.1})$$

The matrix elements of the Hamiltonian in this subspace can be readily calculated from

$$\mathcal{H}_{ij} = \langle e_i | H | e_j \rangle, \quad i, j = 1, 2, \dots, 8. \quad (\text{C.2})$$

For $i \leq j$ the nonzero elements are

$$\begin{aligned} \mathcal{H}_{11} &= E_0 + \omega_1, & \mathcal{H}_{15} &= g_{11}, & \mathcal{H}_{17} &= g_{1a}, \\ \mathcal{H}_{22} &= E_0 + \omega_2, & \mathcal{H}_{26} &= g_{22}, & \mathcal{H}_{27} &= g_{2a}, \\ \mathcal{H}_{33} &= E_0 + \omega_3, & \mathcal{H}_{35} &= g_{31}, & \mathcal{H}_{38} &= g_{3b}, \\ \mathcal{H}_{44} &= E_0 + \omega_4, & \mathcal{H}_{46} &= g_{42}, & \mathcal{H}_{48} &= g_{4b}, \\ \mathcal{H}_{55} &= E_0 + \omega'_1, & \mathcal{H}_{66} &= E_0 + \omega'_2, & \mathcal{H}_{77} &= E_0 + \omega_a, & \mathcal{H}_{88} &= E_0 + \omega_b, \end{aligned} \quad (\text{C.3})$$

whereas the other ones follow by symmetry $\mathcal{H}_{ij} = \mathcal{H}_{ji}$.

2. Second excitation level

We proceed to the second excitation level which has dimension thirty-two. Its basis is chosen as

$$\begin{aligned}
|f_1\rangle &= |2, 0, 0, 0\rangle \otimes |\mathbf{0}, \mathbf{0}\rangle \otimes |\mathbf{0}, \mathbf{0}\rangle, & |f_2\rangle &= |1, 1, 0, 0\rangle \otimes |\mathbf{0}, \mathbf{0}\rangle \otimes |\mathbf{0}, \mathbf{0}\rangle, \\
|f_3\rangle &= |1, 0, 1, 0\rangle \otimes |\mathbf{0}, \mathbf{0}\rangle \otimes |\mathbf{0}, \mathbf{0}\rangle, & |f_4\rangle &= |1, 0, 0, 1\rangle \otimes |\mathbf{0}, \mathbf{0}\rangle \otimes |\mathbf{0}, \mathbf{0}\rangle, \\
|f_5\rangle &= |0, 2, 0, 0\rangle \otimes |\mathbf{0}, \mathbf{0}\rangle \otimes |\mathbf{0}, \mathbf{0}\rangle, & |f_6\rangle &= |0, 1, 1, 0\rangle \otimes |\mathbf{0}, \mathbf{0}\rangle \otimes |\mathbf{0}, \mathbf{0}\rangle, \\
|f_7\rangle &= |0, 1, 0, 1\rangle \otimes |\mathbf{0}, \mathbf{0}\rangle \otimes |\mathbf{0}, \mathbf{0}\rangle, & |f_8\rangle &= |0, 0, 2, 0\rangle \otimes |\mathbf{0}, \mathbf{0}\rangle \otimes |\mathbf{0}, \mathbf{0}\rangle \\
|f_9\rangle &= |0, 0, 1, 1\rangle \otimes |\mathbf{0}, \mathbf{0}\rangle \otimes |\mathbf{0}, \mathbf{0}\rangle, & |f_{10}\rangle &= |0, 0, 0, 2\rangle \otimes |\mathbf{0}, \mathbf{0}\rangle \otimes |\mathbf{0}, \mathbf{0}\rangle \\
|f_{11}\rangle &= |1, 0, 0, 0\rangle \otimes |\mathbf{1}, \mathbf{0}\rangle \otimes |\mathbf{0}, \mathbf{0}\rangle, & |f_{12}\rangle &= |1, 0, 0, 0\rangle \otimes |\mathbf{0}, \mathbf{1}\rangle \otimes |\mathbf{0}, \mathbf{0}\rangle \\
|f_{13}\rangle &= |1, 0, 0, 0\rangle \otimes |\mathbf{0}, \mathbf{0}\rangle \otimes |\mathbf{1}, \mathbf{0}\rangle, & |f_{14}\rangle &= |1, 0, 0, 0\rangle \otimes |\mathbf{0}, \mathbf{0}\rangle \otimes |\mathbf{0}, \mathbf{1}\rangle \\
|f_{15}\rangle &= |0, 1, 0, 0\rangle \otimes |\mathbf{1}, \mathbf{0}\rangle \otimes |\mathbf{0}, \mathbf{0}\rangle, & |f_{16}\rangle &= |0, 1, 0, 0\rangle \otimes |\mathbf{0}, \mathbf{1}\rangle \otimes |\mathbf{0}, \mathbf{0}\rangle \\
|f_{17}\rangle &= |0, 1, 0, 0\rangle \otimes |\mathbf{0}, \mathbf{0}\rangle \otimes |\mathbf{1}, \mathbf{0}\rangle, & |f_{18}\rangle &= |0, 1, 0, 0\rangle \otimes |\mathbf{0}, \mathbf{0}\rangle \otimes |\mathbf{0}, \mathbf{1}\rangle \\
|f_{19}\rangle &= |0, 0, 1, 0\rangle \otimes |\mathbf{1}, \mathbf{0}\rangle \otimes |\mathbf{0}, \mathbf{0}\rangle, & |f_{20}\rangle &= |0, 0, 1, 0\rangle \otimes |\mathbf{0}, \mathbf{1}\rangle \otimes |\mathbf{0}, \mathbf{0}\rangle \\
|f_{21}\rangle &= |0, 0, 1, 0\rangle \otimes |\mathbf{0}, \mathbf{0}\rangle \otimes |\mathbf{1}, \mathbf{0}\rangle, & |f_{22}\rangle &= |0, 0, 1, 0\rangle \otimes |\mathbf{0}, \mathbf{0}\rangle \otimes |\mathbf{0}, \mathbf{1}\rangle \\
|f_{23}\rangle &= |0, 0, 0, 1\rangle \otimes |\mathbf{1}, \mathbf{0}\rangle \otimes |\mathbf{0}, \mathbf{0}\rangle, & |f_{24}\rangle &= |0, 0, 0, 1\rangle \otimes |\mathbf{0}, \mathbf{1}\rangle \otimes |\mathbf{0}, \mathbf{0}\rangle \\
|f_{25}\rangle &= |0, 0, 0, 1\rangle \otimes |\mathbf{0}, \mathbf{0}\rangle \otimes |\mathbf{1}, \mathbf{0}\rangle, & |f_{26}\rangle &= |0, 0, 0, 1\rangle \otimes |\mathbf{0}, \mathbf{0}\rangle \otimes |\mathbf{0}, \mathbf{1}\rangle \\
|f_{27}\rangle &= |0, 0, 0, 0\rangle \otimes |\mathbf{1}, \mathbf{1}\rangle \otimes |\mathbf{0}, \mathbf{0}\rangle, & |f_{28}\rangle &= |0, 0, 0, 0\rangle \otimes |\mathbf{1}, \mathbf{0}\rangle \otimes |\mathbf{1}, \mathbf{0}\rangle \\
|f_{29}\rangle &= |0, 0, 0, 0\rangle \otimes |\mathbf{1}, \mathbf{0}\rangle \otimes |\mathbf{0}, \mathbf{1}\rangle, & |f_{30}\rangle &= |0, 0, 0, 0\rangle \otimes |\mathbf{0}, \mathbf{1}\rangle \otimes |\mathbf{1}, \mathbf{0}\rangle \\
|f_{31}\rangle &= |0, 0, 0, 0\rangle \otimes |\mathbf{0}, \mathbf{1}\rangle \otimes |\mathbf{0}, \mathbf{1}\rangle, & |f_{32}\rangle &= |0, 0, 0, 0\rangle \otimes |\mathbf{0}, \mathbf{0}\rangle \otimes |\mathbf{1}, \mathbf{1}\rangle.
\end{aligned} \tag{C.4}$$

The matrix elements in the second excitation subspace follow analogously as

$$H_{kl} = \langle f_k | H | f_l \rangle, \quad k, l = 1, 2, \dots, 32. \tag{C.5}$$

For the diagonal ones we get

$$\begin{aligned}
H_{11} &= E_0 + 2\omega_1, & H_{22} &= E_0 + \omega_1 + \omega_2, & H_{33} &= E_0 + \omega_1 + \omega_3, & H_{44} &= E_0 + \omega_1 + \omega_4, \\
H_{55} &= E_0 + 2\omega_2, & H_{66} &= E_0 + \omega_2 + \omega_3, & H_{77} &= E_0 + \omega_2 + \omega_4, & H_{88} &= E_0 + 2\omega_3, \\
H_{99} &= E_0 + \omega_3 + \omega_4, & H_{10-10} &= E_0 + 2\omega_4, & H_{11-11} &= E_0 + \omega_1 + \omega'_1, \\
H_{12-12} &= E_0 + \omega_1 + \omega'_2, & H_{13-13} &= E_0 + \omega_1 + \omega_a, & H_{14-14} &= E_0 + \omega_1 + \omega_b, \\
H_{15-15} &= E_0 + \omega_2 + \omega'_1, & H_{16-16} &= E_0 + \omega_2 + \omega'_2, & H_{17-17} &= E_0 + \omega_2 + \omega_a, \\
H_{18-18} &= E_0 + \omega_2 + \omega_b, & H_{19-19} &= E_0 + \omega_3 + \omega'_1, & H_{20-20} &= E_0 + \omega_3 + \omega'_2, \\
H_{21-21} &= E_0 + \omega_3 + \omega_a, & H_{22-22} &= E_0 + \omega_3 + \omega_b, & H_{23-23} &= E_0 + \omega_4 + \omega'_1, \\
H_{24-24} &= E_0 + \omega_4 + \omega'_2, & H_{25-25} &= E_0 + \omega_4 + \omega_a, & H_{26-26} &= E_0 + \omega_4 + \omega_b, \\
H_{27-27} &= E_0 + \omega'_1 + \omega'_2, & H_{28-28} &= E_0 + \omega'_1 + \omega_a, & H_{29-29} &= E_0 + \omega'_1 + \omega_b, \\
H_{30-30} &= E_0 + \omega'_2 + \omega_a, & H_{31-31} &= E_0 + \omega'_2 + \omega_b, & H_{32-32} &= E_0 + \omega_a + \omega_b.
\end{aligned} \tag{C.6}$$

The nonzero matrix elements H_{kl} with $k < l$ are given by

$$\begin{aligned}
H_{1-11} &= \sqrt{2}g_{11}, & H_{1-13} &= \sqrt{2}g_{1a}, \\
H_{2-12} &= g_{22}, & H_{2-13} &= g_{2a}, & H_{2-15} &= g_{11}, & H_{2-17} &= g_{1a}, \\
H_{3-11} &= g_{31}, & H_{3-14} &= g_{3b}, & H_{3-19} &= g_{11}, & H_{3-21} &= g_{1a}, \\
H_{4-12} &= g_{42}, & H_{4-14} &= g_{4b}, & H_{4-23} &= g_{11}, & H_{4-25} &= g_{1a}, \\
H_{5-16} &= \sqrt{2}g_{22}, & H_{5-17} &= \sqrt{2}g_{2a}, \\
H_{6-15} &= g_{31}, & H_{6-18} &= g_{3b}, & H_{6-20} &= g_{22}, & H_{6-21} &= g_{2a}, \\
H_{7-16} &= g_{42}, & H_{7-18} &= g_{4b}, & H_{7-24} &= g_{22}, & H_{7-25} &= g_{2a}, \\
H_{8-19} &= \sqrt{2}g_{31}, & H_{8-22} &= \sqrt{2}g_{3b}, \\
H_{9-20} &= g_{42}, & H_{9-22} &= g_{4b}, & H_{9-23} &= g_{31}, & H_{9-26} &= g_{3b}, \\
H_{10-24} &= \sqrt{2}g_{42}, & H_{10-26} &= \sqrt{2}g_{4b}, & H_{11-28} &= g_{1a}, \\
H_{12-27} &= g_{11}, & H_{12-30} &= g_{1a}, & H_{13-28} &= g_{11}, \\
H_{14-29} &= g_{11}, & H_{14-32} &= g_{1a}, & H_{15-27} &= g_{22}, & H_{15-28} &= g_{2a}, \\
H_{16-30} &= g_{2a}, & H_{17-30} &= g_{22}, & H_{18-31} &= g_{22}, & H_{18-32} &= g_{2a}, \\
H_{19-29} &= g_{3b}, & H_{20-27} &= g_{31}, & H_{20-31} &= g_{3b}, \\
H_{21-28} &= g_{31}, & H_{21-32} &= g_{3b}, & H_{22-29} &= g_{31}, \\
H_{23-27} &= g_{42}, & H_{23-29} &= g_{4b}, & H_{24-31} &= g_{4b}, \\
H_{25-30} &= g_{42}, & H_{25-32} &= g_{4b}, & H_{26-31} &= g_{42}
\end{aligned} \tag{C.7}$$

and those with $k > l$ follow by symmetry $H_{kl} = H_{lk}$.

-
- [1] S.J. Devitt, W.J. Munro, and K. Nemoto, *Quantum error correction for beginners*, Rep. Prog. Phys. **76**, 076001 (2013).
- [2] A.G. Fowler, M. Mariantoni, J.M. Martinis, and A.N. Cleland, *Surface codes: Towards practical large-scale quantum computation*, Phys. Rev. A **86**, 032324 (2012).
- [3] S.B. Bravyi and A.Y. Kitaev, *Quantum codes on a lattice with boundary*, arXiv:[quant-ph]/**9811052** (1998).
- [4] B.M. Terhal, *Quantum error correction for quantum memories*, Rev. Mod. Phys. **87**, 307 (2015).
- [5] R. Versluis, S. Poletto, N. Khammassi, B. Tarasinski, N. Haider, D.J. Michalak, A. Bruno, K. Bertels, and L. DiCarlo, *Scalable quantum circuit and control for superconducting surface code*, Phys. Rev. App. **8**, 034021 (2017).
- [6] Y. Chen, C. Neill, P. Roushan, N. Leung, M. Fang, R. Barends, J. Kelly, B. Campbell, Z. Chen, B. Chiaro, A. Dunsworth, E. Jeffrey, A. Megrant, J.Y. Mutus, P.J.J. O'Malley, C.M. Quintana, D. Sank, A. Vainsencher, J. Wenner, T.C. White, M.R. Geller, A.N. Cleland, and J.M. Martinis, *Qubit architecture with high coherence and fast tunable coupling*, Phys. Rev. Lett. **113**, 220502 (2014).
- [7] T.E. O'Brien, B. Tarasinski, and L. DiCarlo, *Density-matrix simulation of small surface codes under current and projected experimental noise*, npj Quantum Information **3**, 39 (2017).
- [8] L. DiCarlo, J.M. Chow, J.M. Gambetta, L.S. Bishop, B.R. Johnson, D.I. Schuster, J. Majer, A. Blais, L. Frunzio, S.M. Girvin, and R.J. Schoelkopf, *Demonstration of two-qubit algorithms with a superconducting quantum processor*, Nature **460**, 240 (2009).
- [9] Th. K. Mavrogordatos, G. Tancredi, M. Elliott, M.J. Peterer, A. Patterson, J. Rahamim, P.J. Leek, E. Ginossar, and M.H. Szymanska, *Simultaneous bistability of a qubit and resonator in circuit quantum electrodynamics*, Phys. Rev. Lett. **118**, 040402 (2017).
- [10] P. Aliferis and A.W. Cross, *Subsystem fault tolerance with the Bacon-Shor code*, Phys. Rev. Lett. **98**, 220502 (2007).
- [11] H.W.L. Naus and R. Versluis, *Semi-analytical RWA formalism to solve Schrödinger equations for multi-qubit systems with resonator couplings*, arXiv:**1707.02862** [quant-ph] (2017).
- [12] D. Willsch, M. Nocon, F. Jin, H. De Raedt, and K. Michielsen, *Gate-error analysis in simulations of quantum computers with transmon qubits*, Phys. Rev. A **96**, 062302 (2017).
- [13] D. Willsch, M. Willsch, F. Jin, H. De Raedt and K. Michielsen, *Testing quantum fault tolerance on small systems*, Phys. Rev. A **98**, 052348 (2018).
- [14] M.A. Nielsen and I.L. Chuang, *Quantum Computation and Quantum Information*, Cambridge University Press, Cambridge, UK (2000).
- [15] C. Cohen-Tannoudji, B. Diu, F. Laloë, *Quantum Mechanics*, Volume **1**, Wiley-VCH (2005).
- [16] E. Merzbacher, *Quantum Mechanics*, Second Edition, John Wiley & Sons, Inc., New York, (1970).
- [17] C.M. Caves, *Quantum error correction and reversible operations*, Journal of Superconductivity, **12**, 707, (1999).
- [18] H.W.L. Naus, *Four electron spin qubits with exchange interaction*, arXiv:**1905.11181** [quant-ph] (2019).